

1 **Diagnosing uncertainties in global biomass burning emission inventories and**  
2 **their impact on modeled air pollutants**

3 Wenxuan Hua<sup>1,2</sup>, Sijia Lou<sup>1,2,3\*</sup>, Xin Huang<sup>1,2,3</sup>, Lian Xue<sup>1,2,3</sup>, Ke Ding<sup>1,2,3</sup>, Zilin Wang<sup>1,2</sup>,  
4 Aijun Ding<sup>1,2,3</sup>

5 <sup>1</sup> Joint International Research Laboratory of Atmospheric and Earth System Sciences,  
6 School of Atmospheric Sciences, Nanjing University, Nanjing 210023, China.

7 <sup>2</sup> Jiangsu Provincial Collaborative Innovation Center for Climate Change, Nanjing,  
8 China.

9 <sup>3</sup> Frontiers Science Center for Critical Earth Material Cycling, Nanjing University,  
10 Nanjing, China.

11

12 Corresponding author: Sijia Lou ([lousijia@nju.edu.cn](mailto:lousijia@nju.edu.cn))

13

## 14 Abstract

15 Biomass burning (BB) emission inventories are often used to understand the interactions of  
16 aerosols with weather and climate. However, large ~~Large~~ uncertainties ~~exist among~~ persist within  
17 current Biomass burning (BB) inventories, ~~so and~~ the choice of these inventories can greatly  
18 substantially affect ~~impact~~ model results when assessing the influence of BB aerosols on weather  
19 and climate. To quantify the differences among BB emission inventories and reveal their reasons,  
20 ~~we~~ We evaluated discrepancies among BB emission inventories by ~~compared~~ comparing carbon  
21 monoxide (CO) and organic carbon (OC) emissions from seven major BB regions globally ~~from~~  
22 between 2013 to and 2016. The current inventories are based on two basic approaches: (1) bottom-  
23 up approach, which establishes inventories based on observed surface data, and (2) top-down  
24 approach, which based on the release rate of radiative energy from vegetation burning. In this study,  
25 ~~we selected~~ Mainstream bottom-up inventories, including Fire INventory from NCAR 1.5  
26 (FINN1.5) and Global Fire Emissions Database version 4s (GFED4s), and along with the top-down  
27 inventories Quick Fire Emissions Dataset 2.5 (QFED2.5) and VIIRS-based Fire Emission Inventory  
28 version 0 (VFEI0), were selected for this study.

29 ~~We find that~~ The total global CO emissions fluctuate between range from 252 and to 336 Tg, and  
30 the with regional bias is even larger, which can be up to disparities reaching up to a sixfold  
31 difference times. Dry matter is responsible the primary contributor for most of the regional  
32 variation in CO emissions (50-80%), with emission factors accounting for the remaining 20-50%.  
33 Uncertainties in dry matter often come arise from biases in the calculation and of bottom fuel  
34 consumption and burned area, which are closely related to influenced by vegetation classification  
35 methods and fire detection products. In the tropics, peatlands contribute more fuel loads and higher  
36 emission factors than grasslands. At high latitudes, as increased cloud fraction increases, amplifies  
37 the bias discrepancy in between estimated burned area (or fire radiative power) increases by 20%.  
38 In addition, due to the corrected emission factors in QFED2.5, global BB-OC emissions have higher  
39 variability, fluctuating between The global OC emissions range from 14.9 and to 42.9 Tg, exhibiting  
40 higher variability than CO emissions due to the corrected emission factors in QFED2.5, with  
41 regional disparities reaching a factor of 8.7.

42 ~~Finally~~ Additionally, we applied the four sets of these BB emission inventories to the Community  
43 Atmosphere Model version 6 (CAM6) and compared assessed the model results performance with  
44 against observations. Our results suggest that the simulations based on the GFED4s agree best with  
45 the MOPITT-retrieved CO. ~~We also~~ While compared comparing the simulation results with satellite  
46 or ground-based measurments, such as Moderate Resolution Imaging Spectroradiometer (MODIS),  
47 AOD and and AERosol RObotic NETwork (AERONET) aerosol optical depth (AOD), o Our  
48 results reveal that there is no global optimal choice for the BB inventories, In the high latitudes of  
49 the Northern Hemisphere, using GFED4s and QFED2.5 can better capture the AOD magnitude and  
50 diurnal variation. In equatorial Asia, GFED4s outperform others in representing day-to-day changes,  
51 particularly during intense burning. In Southeast Asia, we recommend using the OC emission  
52 magnitude from FINN1.5 combined with daily variability from QFED2.5. In the Southern  
53 Hemisphere, the latest VFEI0 has performed relatively well. but we give certain inventory  
54 recommendations based on different study areas and spatiotemporal scales. This study has  
55 implications for reducing the uncertainties in emissions or improving BB emission inventories in  
56 further studies.

57

| 58

---

|

59

## 60 1 Introduction

61 In recent years, extreme wildfire events have occurred frequently around the world (Balshi et al.,  
62 2009; Knorr et al., 2016; Yang et al., 2019; Jungheun Noyes et al., 2022). The size of the fire has  
63 consistently broken records over the last decades (Westerling et al., 2006; Westerling and Bryant,  
64 2008; Brando et al., 2020), threatened lives and infrastructure, and continuously jeopardized the  
65 global economy. Wildfires are also one of the most important sources of biomass burning (BB)  
66 emissions, which can emit loads of gaseous and particulate pollutants (Ferek et al., 1998; Adams et  
67 al., 2019), detrimental to regional air quality and human health (Reid et al., 2005, Reid and Mooney,  
68 2016). Additionally, BB aerosols, predominantly black carbon (BC) and organic carbon (OC) can  
69 affect regional climate by absorbing/scattering solar radiation, acting as cloud condensation nuclei,  
70 and altering cloud albedo (Spracklen et al., 2011; Boucher et al. 2013). Recent studies have shown  
71 that aerosols produced by biomass burning can significantly affect changes in temperature, cloud  
72 fraction, precipitation, and even the circulation structure (Christian et al., 2019; Yang et al., 2019;  
73 Yu et al., 2019; Carter et al., 2020; Jiang et al., 2020; Ding et al., 2021; Huang et al., 2023). However,  
74 these changes in meteorology are sensitive to the choice of BB emission inventory.

75 ~~Recent studies have shown that aerosols produced by biomass burning can significantly affect~~  
76 ~~changes in temperature, cloud fraction, precipitation, and even the circulation structure (Christian~~  
77 ~~et al., 2019; Yang et al., 2019; Yu et al., 2019; Carter et al., 2020; Jiang et al., 2020; Ding et al.,~~  
78 ~~2021; Huang et al., 2023). Jiang et al. (2020) used the Community Earth System Model version 1.2~~  
79 ~~(CESM1.2) to investigate the impact of BB aerosols on global climate change. They pointed out~~  
80 ~~that BB aerosols reduce the annual mean surface air temperature and precipitation by 0.64 K and~~  
81 ~~0.06 mm day<sup>-1</sup>, respectively. Based on 16 years of simulation from the Weather Research and~~  
82 ~~Forecasting model coupled with Chemistry (WRF-Chem), Ding et al. (2021) reported that BB~~  
83 ~~aerosols increased low cloud coverage by 20% in areas downwind of wildfires in Southeast Asia in~~  
84 ~~March and Southern Africa in August. A recent study also reported that the radiative effects of BB~~  
85 ~~aerosols alter the local circulation structure, leading to dry air on the West Coast of the United States,~~  
86 ~~or less precipitation in Southeast Asia, thus intensifying fires and exacerbating air pollution (Huang~~  
87 ~~et al., 2023). However, these simulated results are sensitive to the amount of BB pollutants (Liu et~~  
88 ~~al., 2020a).~~

89 —Previous studies often found that there is a significant deviation between the gaseous or  
90 particulate pollutants simulated by the model and the satellite retrieval value (Bian et al., 2007;  
91 Chen et al., 2009; Carter et al., 2020), one of the most important reasons comes from the  
92 uncertainties in emission inventories. For example, Bian et al. (2007) applied six different BB  
93 emission inventories, GFED1 and GFED2 (Global Fire Emissions Database version 1 and 2)  
94 (GFED1 and GFED2), Arellano1, Arellano2, Duncan1, and Duncan2, to the Unified Chemistry  
95 Transport Model (UCTM). They reported that although the total global CO of the six BB emission  
96 inventories was within 30% of each other, the model results suggested that regional deviations can  
97 be much higher, by as much as 2-5 times, especially in the Southern Hemisphere. Bias in emission  
98 inventories can therefore often have a significant impact on the direct and indirect effects of models  
99 on aerosol assessments (Liu et al., 2018; Liu et al., 2020a; Ramnarine et al., 2019; Carter et al.,  
100 2020). Carter et al. (2020) compared the simulated black carbon (BC) and organic carbon (OC)  
101 concentrations with measurements from IMPROVE (Interagency Monitoring of Protected Visual  
102 Environments) observation network from May to September. They suggested that using the

103 FINN1.5 inventory (Fire INventory from NCAR 1.5) improves model results in eastern North  
 104 America, while using GFED4s, QFED2.4 (Quick Fire Emissions Dataset 2.4), and GFAS1.2 (Global  
 105 Fire Assimilation System 1.2) inventories shows better agreement with observations in western  
 106 North America. They also noted that population-weighted BB PM<sub>2.5</sub> concentrations in Canada and  
 107 the adjacent United States could vary between 0.5 and 1.6 μg m<sup>-3</sup> in 2012 by using different BB  
 108 emissions. Liu et al. (2018) used the global model CAM5 (The Community Atmosphere Model 5)  
 109 and three different BB emission inventories to analyze the uncertainties in the aerosol radiative  
 110 effects in the Northeastern United States in early April 2009. They found that aerosols exhibited a  
 111 stronger cooling effect when CAM5 used the QFED2.4 inventory than the GFED3.1 and GFED4s  
 112 inventories, with additional cooling of -0.7 W m<sup>-2</sup> and -1.2 W m<sup>-2</sup> through aerosol direct radiative  
 113 effect and the aerosol-cloud radiative effect, respectively. On a global basis, Ramnarine et al. (2019)  
 114 used the global model GEOS-Chem-TOMAS (GEOS-Chem-Two-Moment Aerosol Sectional), and  
 115 found that the direct radiative effects and indirect effects of aerosols driven by the FINN1.5 emission  
 116 inventory in 2010 were 70% and 10% lower than those driven by GFED4, respectively. Therefore,  
 117 to better estimate regional aerosol-radiation/aerosol-cloud interactions in wildfire regions, it is  
 118 necessary to understand the differences in emission inventories from biomass combustion and the  
 119 main drivers of uncertainties.

120 In general, BB emission inventories are based on bottom-up or top-down methods to infer the  
 121 emission source intensity. The bottom-up approach, also known as the fire detection and/or burned  
 122 area method, estimates emissions based on surface data such as fuel loading, active fire counts,  
 123 and/or burned area. Currently, the widely used BB inventories based on the bottom-up approach  
 124 include Duncan (Duncan, 2003), GFED (van der Werf et al., 2006, 2010a, 2010b, 2017), FINN  
 125 (Wiedingmyer et al., 2011), Global Inventory for Chemistry-Climate Studies-GFED4S (G-G)  
 126 (Mieville et al., 2010). The top-down approach uses satellite observations of fire radiative power  
 127 (FPR), a method to measure the radiative energy release rate of burning vegetation, to estimate  
 128 emissions by fuel consumption. The BB inventories based on the top-down method include Arellano  
 129 (Arellano Jr et al., 2004; Arellano Jr and Hess, 2006), GFAS (Kaiser et al., 2012), Fire Energetics  
 130 and Emission Research (FEER) (Ichoku and Ellison, 2014), QFED (Darmenov et al., 2015), the  
 131 Fire Emissions Estimate Via Aerosol Optical Depth (FEEV-AOD) (Paton-Walsh et al., 2012) and  
 132 the recently released VIIRS-based Fire Emission Inventory version 0 (VFEI0) (Ferrada et al., 2022).  
 133 On a global scale, the average annual BB emissions of CO and OC can differ by a factor of 3 to 4,  
 134 with the global emissions fluctuating in the range of 280-580 Tg yr<sup>-1</sup> and 13-50 Tg yr<sup>-1</sup> respectively.  
 135 The bias may be even greater when focusing on emissions in specific regions (Bian et al., 2007;  
 136 Lioussse et al., 2010; Williams et al., 2012; Carter et al., 2020; Lin et al., 2020b; Liu et al., 2020b).  
 137 For example, the estimated CO emission of Arellano inventory in South America during the burning  
 138 peak season of September 2000 is four times greater than that of GFED1 inventory (Bian et al.,  
 139 2007). A recent study even found that since 2008, OC emissions from QFED2.5 in the Middle East  
 140 are approximately 50 times larger than those from GFED3 and GFED4 (Pan et al., 2020).

141 Several previous studies have analyzed the reason for the huge emission bias. According to  
 142 Darmenov et al. (2015), the emissions E<sub>i</sub> (mass of pollutant i) is the sum of the products of the  
 143 emission factor (EF<sub>b</sub>) and the dry matter (DM<sub>b</sub>) for each biome:

$$144 \quad E_i = \sum_b EF_b \times DM_b \quad (1)$$

145 While earlier studies suggested that the uncertainty in BB emissions arises mainly from differences  
 146 in emission factors (e.g., Alvarado et al., 2010; Akagi et al., 2011; Urbanski et al., 2011), more

147 recent studies point out that uncertainty in dry matter also plays an important role ~~in differences in~~  
 148 ~~BB emissions~~ (Paton-Walsh et al., 2010; 2012; Carter et al., 2020). For example, Paton-Walsh et al.  
 149 (2012) assessed the difference in CO emissions from the February 2009 Australian fire and found  
 150 that total CO emissions in GFED3.1 were roughly three times higher than that in FINN1, with DM  
 151 contributing up to 80%. Carter et al. (2020) evaluated emissions from various North American BB  
 152 inventories over the period 2004-2016 and found that changes in DM ~~was-were~~ very close to the  
 153 emission trend, suggesting that uncertainty in potential DM across ~~the~~ North American was the  
 154 primary factor, rather than EF.

155 The accuracy of BB inventories is influenced by IEF.

156 ~~—To analyze the root causes of the differences in EFs and DM among BB inventories, equation~~  
 157 ~~(1) is further decomposed. According to the bottom up method, the emission for each species i can~~  
 158 ~~be further summarized as:~~

$$159 \quad E_t = \sum_b (EF_b \times BA(x,t) \times FC_b) = \sum_b (EF_b \times BA(x,t) \times FL_b \times FB_b) \quad (2)$$

160 where BA(x,t) is burned area at location x and time t, which can be obtained from the fire  
 161 detection products. For each biome, fuel consumption (FC<sub>b</sub>) is the product of fuel loadings (FL<sub>b</sub>)  
 162 and the fraction of biomass burned (FB<sub>b</sub>), which can be obtained with reference to static biomass  
 163 density or using a biological models.

164 Similarly, the top-down inventories can be further divided into:

$$165 \quad E_t = \sum_b A \times FRP/A \times \alpha_i \quad (3)$$

166 where A is the area of unit pixel observed by satellite, and FRP/A represents the FRP density,  
 167 which is proportional to E<sub>i</sub>. For the emission E<sub>i</sub> of a substance i, the empirical coefficient α<sub>b</sub> is used  
 168 to convert the fire radiative energy (i.e., the time-integrated FRP) of each biome into DM (also can  
 169 be considered as converting FRP density into emission fluxes).

170 ~~—Therefore, land cover and land use (LULC) data, associated with vegetation types can~~  
 171 ~~influence the BB inventory by impacting both affecting EFs and EFs, fuel loads, and the FB for~~  
 172 ~~bottom-up approach, or by affecting EFs and empirical coefficient α for top-down approach DM~~  
 173 ~~(Wiedinmyer et al., 2006; Ferrada et al., 2022). In a study by For example, Wiedinmyer et al. (2006),~~  
 174 ~~used three different-distinct LULC products were employed to drive a regional model of BB~~  
 175 ~~emissions model. and found that The variations inying LULC products drive-led through-to~~  
 176 ~~discrepancies in fuel consumption, ultimately-leading-to-resulting in an annual bias of up to 26% in~~  
 177 ~~North and Central America. Furthermore/Moreover, since EFs are highly-dependent/closely tied on~~  
 178 ~~to various-different biomes, different biome-classifications-will introducinge uncertainty into BB~~  
 179 ~~emission inventories with varied biome classifications~~ (Ferrada et al., 2022). In addition to LULC  
 180 products, uncertainties are introduced by fire detection products (such as FRP and burned area  
 181 products) that are, affected by factors such as satellite transit time and cloud obscuration ~~also bring~~  
 182 ~~uncertainty to BB emission inventories~~. For example, Paton-Walsh et al. (2012) found that in an  
 183 Australian fire called "Black Friday" in February 2009, the burned areas of FINN1 were barely half  
 184 of that of GFED3.1. Liu et al. (2020b) reported that compared with the active fire area used in  
 185 FINN1.5, the burned area product selected by GFED4s is less sensitive to the satellite overpass time  
 186 and cloud obscuration. These results indicate that LULC and fire detection products are key factors  
 187 leading to bias in BB emission estimation.

188 Although previous work has generated biomass burning emission inventories and attempted to  
 189 reduce their uncertainties (Duncan, 2003; Arellano Jr et al., 2004; Arellano Jr and Hess, 2006; van  
 190 der Werf et al., 2006, 2010a, 2010b, 2017; Bian et al., 2007; Mieville et al., 2010; Wiedingmyer et

191 al., 2011; Kaiser et al., 2012; Paton-Walsh et al., 2012; Ichoku and Ellison, 2014; Darmanov et al.,  
192 2015; Liu et al., 2018; Ramnarine et al., 2019; Carter et al., 2020; Lin et al., 2020b; Liu et al., 2020b;  
193 Pan et al., 2020; Zhang et al., 2020; Ferrada et al., 2022), they did not analyze the reasons why DM  
194 and EF exhibited large differences among various emission inventories, which may vary over time  
195 and location. Here, this study aims to explore the underlying reasons for the differences in BB  
196 emission inventories in major combustion regions around the world, thereby attempting to reduce  
197 the uncertainties of the impact of BB emission inventories on model results. To minimize the  
198 interference of anthropogenic emissions on model results, we selected combustion regions  
199 satisfying the following conditions: (1) regional BB CO emissions above 20 Tg yr<sup>-1</sup>; (2) BB CO  
200 emissions contribute more than 70% of the total. We ultimately selected seven major burning areas  
201 as shown in Fig. 1, including Boreal North America (BONA), Southern Hemispheric South America  
202 (SHSA), Northern Hemispheric Africa (NHAF), Southern Hemispheric Africa (SHAF), Boreal Asia  
203 (BOAS), Southeast Asia and India (SEAS), and Equatorial Asia (EQAS).

204 ~~Due to the abundance of published BB inventories, in this study~~In this study, we compare several  
205 ~~widely used datasets we selected several datasets that are widely used~~ (FINN1.5, GFED4s, and  
206 QFED2.5) and the ~~latest-recently~~ released VFEI0. ~~for comparison, with~~ ~~†~~The former two ~~of~~  
207 ~~the datasets are~~ based on ~~the~~ bottom-up method, ~~and while~~ the ~~latter two others are~~ based on ~~the~~  
208 top-down method. Specific details of ~~these~~ BB inventories ~~will be~~ ~~are~~ described in Section 2. In  
209 section 3.1, we ~~will discuss~~ ~~explore~~ the differences ~~of in~~ CO and OC emissions among ~~the~~ four  
210 inventories, ~~along with~~ ~~examining~~ the contributions of DM and EFs to ~~these~~ differences,  
211 respectively. For the first time, we ~~have~~ evaluated the biases of CO column concentrations and AOD  
212 driven by BB ~~inventories~~ in the CESM2-CAM6 model. ~~Based on our findings, and given we~~  
213 ~~provide recommendations suggestions~~ on ~~what which~~ inventory should be adopted across various  
214 regions. ~~(Section 3.2). Section 4 presents~~ ~~†~~The conclusion and discussion ~~are presented in section 4,~~  
215 and our research is ~~anticipated expected~~ to ~~provide some offer~~ insights ~~for into~~ reducing the  
216 uncertainties ~~of with~~ BB emission datasets.

217

## 218 2 Data and Methodology

### 219 2.1 Biomass Burning emission inventories

220 We simultaneously diagnosed the differences ~~among between~~ two bottom-up approach  
221 inventories and two top-down approach inventories, including FINN1.5, GFED4s, and QFED2.5,  
222 which are commonly used in the current atmospheric model, as well as the recently released VFEI0.  
223 Details about the emission inventories and the satellite products they use are listed in Table 1 ~~and~~  
224 ~~Text S1 in supplementary.~~

225

#### 226 Bottom-up (Burned Area) inventories

227 ~~Among the four BB emission inventories selected in this study, both~~ FINN1.5 and GFED4s ~~both~~  
228 ~~use adopt~~ ~~the a~~ bottom-up ~~method approach~~, ~~also known as the~~ ~~(also called the~~ Burned Area method),  
229 ~~and the.~~ ~~As shown~~ ~~details are shown~~ in Table 1, FINN1.5 uses the MODIS (Moderate Resolution  
230 Imaging Spectroradiometer) product MCD14DL ~~to for~~ ~~calculate the~~ burned area ~~calculations.~~  
231 ~~which can monitor fire points with an area larger than 0.05 km<sup>2</sup>. Since the MCD14DL is an~~ ~~This~~  
232 active fire detection product ~~monitors real-time fire points larger than 0.05 km<sup>2</sup> that reflects real-~~  
233 ~~time fire point detectio.~~ ~~However, it is important to note that,~~ if a fire occurs ~~but when~~ the satellite

234 is not in transit or is obscured by clouds ~~while the satellite is in during~~ transit, ~~the fire~~ it will not be  
235 detected (Firms, 2017). Additionally, ~~considering that MODIS on polar orbiting satellites cannot~~  
236 ~~provide daily coverage products in the tropics (30°N-30°S)~~, FINN1.5 ~~makes some smoothing~~  
237 ~~assumptions for fire detection in this region. It~~ assumes that every fire detected at the equator (~~30°N-~~  
238 ~~30°S~~) will ~~continue-persist~~ the next day at half the size of the previous day (Table 1), ~~and However,~~  
239 this assumption ~~obviously raises some questions~~ may not accurately reflect real-world conditions  
240 (Wiedinmyer et al., 2011; Pan et al., 2020). ~~Meanwhile,~~ ~~†~~The ~~land cover~~ classification ~~of land cover~~  
241 ~~types~~ in FINN1.5 is based on MCD12Q1 (IGBP, version 2005). According to the IGBP land cover  
242 classification, each fire is initially assigned to one of 16 land use/land cover (LULC) classes, and  
243 then lumped into six generic categories including tropical forest, temperate forest, boreal forest,  
244 savanna and grasslands, woody savannas and shrublands, and cropland (Fig. S1, Wiedinmyer et  
245 al., 2011). ~~The amount of usable biomass that can be burned per fire (fuel loadings) for each generic~~  
246 ~~LULC according to Hoelzemann et al. (2004). The FB for each fire is specified as a function of~~  
247 ~~vegetation cover (MODIS Vegetation Continuous Fields (VCF) product), as described by~~  
248 ~~Wiedinmyer et al. (2006; 2011).~~ Emission factors (EFs) for various gaseous and particulate species  
249 are determined from a dataset compiled by Akagi et al. (2011) and Andreae and Merlet (2001), ~~and~~  
250 ~~with~~ these EFs ~~varying~~ for different LULC types. Currently, FINN1.5 provides ~~the~~ daily global  
251 emissions from biomass burning since 2002, including 41 species, with a spatial resolution of 1 km<sup>2</sup>  
252 (Table 1).

253 ~~The main difference between FINN1.5 and GFED4s differs in that it primarily is that the latter~~  
254 ~~mainly uses the MCD64A1 Collection 5.1 burned area product (Giglio et al., 2013; Randerson et~~  
255 ~~al., 2018), which can only capable of detecting fires with a size larger than 500 m × 500 m. For small~~  
256 ~~fire burning areas, GFED4s additionally incorporate active fire detection products (MOD14A1 and~~  
257 ~~MYD14A1), and by comparing the difference normalized burned area (dNBR) of active fire~~  
258 ~~products observed inside and outside the 500 m burning area, which compensates~~ to some extent  
259 for the ~~bias caused by the~~ lower spatial resolution of the original product MCD64A1 (van der Werf  
260 et al., 2017). ~~Note that, according to van der Werf et al. (2017), only small or moderate angle fire~~  
261 ~~point detections are retained in order to reduce uncertainty in geolocation.~~ In general, burned area  
262 products reduce uncertainty in fire detection due to satellite non-transit and cloud/smoke  
263 obscuration when ~~a~~ burn occurs by identifying day-to-day surface variations, such as charcoal and  
264 ash deposition, vegetation migration, and changes in vegetation structure (Boschetti et al., 2019).  
265 ~~Similar to FINN1.5, each fire in GFED4s is initially assigned to one of 16 LULC subcategories and~~  
266 ~~then lumped into six categories, with the inclusion of an additional biome, peatland (Fig.~~  
267 ~~S1).~~ According to the annual MODIS MCD12C1 version 5.1 land cover type product and University  
268 of Maryland (UMD) classification scheme (Friedl et al., 2010), each fire is also initially assigned to  
269 one of 16 LULC subcategories and then lumped into six categories: tropical forest, temperate forest,  
270 boreal forest, savanna, cropland (agriculture), and peatland as shown in Fig. S1. While GFED4s  
271 combines the “savanna and grasslands” and “woody savannas and shrublands” in FINN1.5 into one  
272 biome, it has an additional biome “peatland”. GFED4s generate the fuel loadings and the fraction  
273 of biomass burned for each category by combining the burned area and vegetation mortality in a  
274 modified Carnegie Ames Stanford Approach (CASA) model, which is driven by the data of  
275 temperature, precipitation, solar radiation, NDVI, and vegetation types (Schaefer et al., 2008; van  
276 der Werf et al., 2010; 2017). Additionally, EFs for various ~~gaseous and particulate~~ species follow  
277 Akagi et al. (2011) and Andreae and Merlet (2001), ~~also varying across with~~ different biome



278 categories. Currently, GFED4s provides ~~the~~ daily global emissions from biomass burning since  
279 1997, including 27 species, with a spatial resolution of  $0.25^\circ \times 0.25^\circ$  (Table 1). However, since 2017,  
280 the DM provided by GFED4s is derived from a linear relationship between past emissions and  
281 MODIS FRP data for the period 2003–2016.

282

## 283 **Top-down (Fire Radiative Power) inventories**

284 ~~The other two emission inventories selected for~~In this study, both QFED2.5 and VFEI0<sub>7</sub> use a  
285 top-down approach, ~~also~~ known as the Fire Radiative Power (FRP) method. ~~Unlike~~ In contrast to  
286 the bottom-up approach, the top-down approach ~~is not based~~ relies on satellite products detecting  
287 fire-radiated power rather than on fire point detection, ~~but on satellite products that detected fire~~  
288 radiated power. QFED2.5 uses MODIS Collection 6 MOD14/MYD14 level 2 products to estimate  
289 the fire radiative power, and pinpoint fire locations using MOD03/MYD03 ~~to pinpoint the location~~  
290 of the fire (Darmenov and Silva 2015; Liu et al., 2020b). ~~Since MOD14 and MYD14 products are~~  
291 strongly influenced by clouds, missing FRPs are corrected using the "sequential approach"  
292 combining current observations and predicted values (Darmenov and da Silva, 2015). The FRPs are  
293 ~~then~~ integrated in-over time to obtain ~~the~~ fire radiative energy (FRE), which is ~~detected and~~  
294 converted to DM by using an empirical coefficient  $\alpha$ . The initial ~~value of  $\alpha$  values in QFED2.5 is~~  
295 taken obtained from Kaiser et al. (2009) and ~~subsequently are~~ adjusted monthly based on global  
296 emissions of GFED2 in 2003–2007, ~~resulting in two sets of empirical coefficients:  $\alpha_{\text{MOD14}} = 1.89 \times$~~   
297  ~~$10^{-6} \text{ kg (DM) J}^{-1}$  and  $\alpha_{\text{MYD14}} = 0.644 \times 10^{-6} \text{ kg (DM) J}^{-1}$~~ . In QFED2.5 classifies land cover using,  
298 the International Geosphere-Biosphere Programme (IGBP-INPE) dataset, ~~classes are used to~~  
299 aggregating 17 land cover classes into four broad vegetation types, ~~including tropical forest, extra-~~  
300 ~~tropical forest (forest classes that exclude tropical forest), savanna, and grassland~~ (Fig. S1,  
301 Darmenov and da Silva 2015). Initially, EFs for various species in QFED2.5 also follow Akagi et  
302 al. (2011) and Andreae and Merlet (2001) ~~The EFs of particulate or trace gas species are from~~  
303 ~~previous studies (Andreae and Merlet, 2001; Akagi et al., 2011)~~. But for certain species, including  
304 organic carbon (OC), black carbon (BC), ammonia (NH<sub>3</sub>), sulfur dioxide (SO<sub>2</sub>), and particulate  
305 matter diameter < 2.5  $\mu\text{m}$  (PM<sub>2.5</sub>), QFED2.5 incorporates a scaling factor to enhance the EFs.  
306 QFED2.5 provides daily global BB emissions since 2000, including 17 species, with a spatial  
307 resolution of  $0.1^\circ \times 0.1^\circ$  (Table 1).

308 ~~It is important to note that QFED2.5 scales up the EFs for emissions associated with the particulate~~  
309 ~~phase, such as organic carbon (OC), black carbon (BC), ammonia (NH<sub>3</sub>), sulfur dioxide (SO<sub>2</sub>), and~~  
310 ~~particulate matter diameter < 2.5  $\mu\text{m}$  (PM<sub>2.5</sub>), so emissions of these species are greater in QFED2.5~~  
311 ~~than in other inventories. The QFED2.5 product covers daily emission inventories from 2000 to the~~  
312 ~~present, and contains 17 emission species with a spatial resolution of up to  $0.1^\circ \times 0.1^\circ$ .~~

313 VFEI0 also adopts the top-down method but uses VNP14IMG.001 FRP product from VIIRS I-  
314 band (Visible Infrared Imaging Radiometer), This product has a higher resolution (375 m at nadir)  
315 compared to MODIS (1 km resolution at nadir), enabling the detection of which can detect smaller  
316 and colder flames than MODIS (1 km resolution at nadir), since it has a resolution of 375 m at nadir  
317 (Ferrada et al., 2022). ~~Unlike QFED2.5, VFEI0 has no cloud calibration, but it will be supplemented~~  
318 in future versions. It also uses the an empirical coefficient  $\alpha$  derived from the linear regression of  
319 GFED3.1 DM and VIIRS FRP to convert ~~the~~ detected FRE into DM, ~~but  $\alpha$  is derived from the linear~~  
320 regression of GFED3.1DM and VIIRS FRP. Additionally, VFEI0 uses MCD12C1 (IGBP, version

2015) ~~is as~~ the underlying LULC data, ~~which is further~~ supplemented by Köppen climate classification (Beck et al., 2018), ~~to define~~ ten subcategories in VFEI0 (~~i.e., Tropical forest, Savanna, Temperate forest, Temperate Savanna, Boreal forest, Boreal Savanna, Grass, Agriculture, Peatland and Desertic areas~~ Fig. S1). VFEI0 ~~then grouped the previous ten~~ these subcategories into six biomes (Fig. S1), corresponding to ~~the emission factors~~ EFs provided by Andreae (2019), ~~to calculate the BB emission inventory. Among the four BB emission inventories~~ Currently, VFEI0 ~~provides offers the shortest inventory time coverage (daily BB emission fluxes from since 20 January 2012 to the present), but it provides the largest number of emitted species at covering 46 emitted species with~~ and the highest a horizontal resolution of  $0.005^\circ \times 0.005^\circ$  (Table 1).

## 2.2 The calculation for EFs and DMs

To calculate regional EFs and DMs, we adopt the approach outlined by Carter (2020). Initially, we divide CO emissions per grid by the EF applied to each biome, yielding DM:

$$DM_{b,x} = CO_{b,x} / EF_b \quad (1)$$

where b represents one of the seven biomes in Fig. S1, and x represents the location grid. This calculation of DM using CO is reasonably representative, given that the inventories are not adjusted for CO emission factors. After calculating  $DM_{b,x}$  for each grid, we derive a regional average emission factor by dividing total CO emissions by total DM for each major BB region:

$$EF_{CO} = \sum_{b,x} CO / \sum_{b,x} DM \quad (2)$$

These calculations enable us to discern the influence of LULC classification on BB emission inventories. For a specific biome type within a given region, we calculate EF by dividing the CO emissions of that particular biome classification by the sum of the value from each biome in the respective region:

$$EF_b = CO_b / \sum_b DM \quad (3)$$

where b represents one of the seven biome classifications in this study (Fig. S1).

Furthermore, for the two bottom-up inventories, we invert the fuel consumption for each vegetation biome b within a given area:

$$FC_b = DM_b / BA \quad (4)$$

Here, the DM corresponding to each biome in FINN1.5 and GFED4s is obtained using equation (1), and BA represents the total burned area derived from the emission inventory.

## 2.2.3 Quantitative statistical methods

As described in section 2.1, fire detection is greatly affected by cloud/smoke obscuration in the bottom-up approach. For example, if there are clouds/smoke at high altitudes while fire occurs on the ground, the MCD14DL active fire detection product used in FINN1.5 may miss these fire points. In addition, ~~for~~ the combustion that is too small in size and too low in temperature, ~~it~~ cannot be effectively monitored due to the low brightness temperature contrast with the surrounding environment. In contrast, the burned area product (mainly MCD64A1) used by GFED4s determines the burning information based on the changes such as surface albedo, and is, therefore less affected by clouds/smoke. For inventories based on the top-down approach, the emission inventories also differ to a large extent due to the cloud/smoke obscuration, since QFED2.5 uses a “sequential method” to correct for missing FRPs during cloud/smoke obscuration, whereas VFEI0 does not. Thus, in this study, the symmetrical mean absolute percentage error (SMAPE) and Pearson's R are

364 used to ~~access~~ assess the difference in sensitivity to clouds/smoke between the two BB products  
365 based on the bottom-up (or top-down) approach. The specific algorithm is as follows:

$$366 \quad \text{SMAPE} = \frac{100\%}{n} \sum_{i=1}^n \frac{|X-Y|}{(|X|+|Y|)/2}, \quad (45)$$

$$367 \quad R = \frac{\sum_{i=1}^N (X-\bar{X}) \cdot (Y-\bar{Y})}{\sqrt{\sum_{i=1}^N (X-\bar{X})^2 \cdot \sum_{i=1}^N (Y-\bar{Y})^2}}, \quad (56)$$

368 where X and Y are fire detection data from two different datasets (e.g. burned area from FINN1.5  
369 and GFED4s or FRP from VFEI0 and QFED2.5). We divided these fire detection data into three  
370 groups according to the cloud fractions less than 0.4, 0.4-0.7, and greater than 0.7, and the number  
371 n represents valid samples in different cloud fraction groups. SMAPE ranges from 0% to 200%,  
372 with smaller values indicating smaller differences, while Pearson's R ranges from 0 to 1, with  
373 smaller values implying less correlation.

374 In order to quantify the effect of cloud obscuration on BB datasets, we selected the most intensely  
375 burning regions in BONA in July for this study. For consistency, we re-interpolated the fire  
376 detection data used in the four BB datasets, as well as the MODIS MCD06 cloud fraction data, to  
377 the same horizontal resolution ( $0.25^\circ \times 0.25^\circ$ ). Considering the continuity of combustion, we took  
378 every  $5^\circ \times 5^\circ$  as a sample area in the northern U.S. to ensure that if a large burn occurred, the area  
379 would be detected to some extent, avoiding errors due to differences between the inventories. At  
380 the same time, we excluded the samples ~~in~~ at the same time and location, where the emissions are  
381 all zero. Finally, a total of 1888 samples were obtained for the burned area group, with 534, 541,  
382 and 813 samples for low ( $<0.4$ ), medium (0.4-0.7), and high ( $>0.7$ ) cloud fraction, respectively. A  
383 total of 1,682 samples were obtained for the FRP group, with 860, 390, and 432 samples under low,  
384 medium, and high cloud fraction, respectively. It is worth noting that we use the average FRP of  
385 MOD and MYD for QFED2.5 since the VFEI0 FRP is the average between day and nighttime  
386 observations. Moreover, our approach cannot rule out the case of missing measurements when two  
387 sets of BB inventories are both obscured by the cloud. However, the main goal of this paper is to  
388 explore the causes of uncertainties in emission inventories, the specific case of omission due to  
389 cloud obscuration depends on the development of satellite detection technology and is not part of  
390 the purpose of this study.

### 392 **2.3.4 CSM2-CAM6 model**

393 The Community Earth System Model version 2.1 (CESM2) is a new generation of the coupled  
394 climate/Earth system models developed by National Center for Atmospheric Research (NCAR). In  
395 this study, we used the global Community Atmosphere Model version 6 (CAM6) (Danabasoglu et  
396 al., 2020). Gas-phase chemistry was represented by the Model for Ozone and Related chemical  
397 Tracers tropospheric chemistry (MOZART-T1, Emmons et al., 2020). The wet deposition of soluble  
398 gaseous compounds in CAM6-Chem is based on the scheme of Neu and Prather (2012), which  
399 describes the process of in-cloud cleaning and under-cloud cleaning. The formation of secondary  
400 organic aerosols (SOA) is from a volatility basis set (VBS) approach developed by Tilmes (2019).  
401 Properties and processes of aerosol species of black carbon (BC), primary organic aerosols (POA),  
402 SOA, sulfate, dust, and sea salt are calculated by Modal Aerosol Module (MAM4) described by Liu  
403 (2016). CAM6 uses a horizontal resolution of nominal  $1^\circ$  ( $1.25^\circ \times 0.9^\circ$ -, longitude by latitude) and  
404 32 vertical levels from the surface to 2.26 hPa ( $\sim 40$  km).

405 In this study, four BB emission inventories (FINN1.5, GFED4s, QFED2.5, and VFEI0) are re-  
406 gridded to a horizontal resolution of  $1.25^\circ$  (longitude)  $\times$   $0.9^\circ$  (latitude), and then applied to the  
407 model. All simulations were performed for five years, while horizontal winds and temperature ~~are~~  
408 ~~were~~ nudged toward the Modern-Era Retrospective analysis for Research and Applications, version  
409 2 (MERRA-2) reanalysis data (GMAO, 2015) for every 6 h. Simulations are conducted for 2012-  
410 2016, with the first year used for initialization and model spin-up. Daily BB emissions were applied  
411 in this study, whereas the vertical distribution of fire emissions was followed Freitas et al. (2006,  
412 2010). Anthropogenic and biogenic emissions in this study are from the Community Emissions Data  
413 System (CEDS) and Model of Emissions of Gases and Aerosols from Nature version 2.1  
414 (MEGANv2.1), respectively, at 2010 levels (Guenther et al., 2012; Hoesly et al., 2018).

## 416 **2.4.5 Measurement data**

417 The Tropospheric Pollution Measurement Instrument (MOPITT) is aboard the Earth Observing  
418 System (EOS)/Terra satellite launched by NASA (Warner, et al., 2001). MOPITT is the first  
419 instrument to observe the global concentration and currently provides column concentration and  
420 volume mixing ratio of global carbon monoxide (CO) since 1999. We used MOPITT CO gridded  
421 monthly means (Near and Thermal Infrared Radiances) V009 (MOP03JM\_9; NASA Langley  
422 Atmospheric Science Data Center DAAC, retrieved from  
423 <https://doi.org/10.5067/TERRA/MOPITT/MOP03JM.009>), which has a horizontal resolution of  $1^\circ$   
424  $\times$   $1^\circ$ . It should be noted that ~~in order~~ to compare the CO column concentration simulated by CESM2-  
425 CAM6 with MOPITT CO, we calculated the simulated CO column concentrations by cumulative  
426 integration from 900 hPa to 100 hPa isobaric height (Deeter et al., 2022). We also used the daily  
427 AOD (550 nm) and cloud fraction data from MODIS products MOD08\_D3 (MODIS/Terra Aerosol  
428 Cloud Water Vapor Ozone Daily L3; Platnick et al. 2015) and MCD06COSP (MODIS (Aqua/Terra)  
429 Cloud Properties Level 3 daily, Webb et al., 2017), respectively.

430 The observations of AERONET (<http://AERONET.gsfc.nasa.gov/>; Holben et al., 1998) from 12  
431 sites are used in this study. These AERONET stations were selected since they are close to BB  
432 source regions. As marked in Figure 1b, these sites include sites in BONA (Yellowknife\_Aurora  
433 ( $62.5^\circ\text{N}$ ,  $114.4^\circ\text{W}$ ), Pickle Lake ( $51.4^\circ\text{N}$ ,  $90.2^\circ\text{W}$ )), BOAS (Tiksi ( $71.6^\circ\text{N}$ ,  $128.9^\circ\text{E}$ ), Yakutsk  
434 ( $61.7^\circ\text{N}$ ,  $129.4^\circ\text{E}$ )), SHAF (Namibe ( $15.2^\circ\text{S}$ ,  $12.2^\circ\text{E}$ ), Mongu Inn ( $15.3^\circ\text{S}$ ,  $23.1^\circ\text{E}$ )), SHSA (Alta  
435 Floresta ( $9.9^\circ\text{S}$ ,  $56.1^\circ\text{W}$ ), Rio Branco ( $9.9^\circ\text{S}$ ,  $67.9^\circ\text{W}$ )), EQAS (Palangkaraya ( $2.2^\circ\text{S}$ ,  $113.9^\circ\text{E}$ ),  
436 Jambi ( $1.6^\circ\text{S}$ ,  $103.6^\circ\text{E}$ )), SEAS (Omkoi ( $17.8^\circ\text{N}$ ,  $98.4^\circ\text{E}$ ), Ubon Ratchathani ( $15.2^\circ\text{N}$ ,  $104.9^\circ\text{E}$ )).

437 All observed AOD represent real atmospheric conditions and therefore, in addition to BB aerosols,  
438 biogenic aerosols, anthropogenic aerosols, dust, and sea salts are also integrated in MODIS and  
439 AERONET datasets.

## 441 **3 Comparative analysis of emission inventories**

442 CO and OC are the main species emitted from biomass burning (Westerling et al., 2010; van der  
443 Werf et al., 2010b; Carter et al., 2020) but emissions vary widely. In this study, we compare the  
444 differences in CO and OC emissions (representing gaseous and particulate pollutants, respectively)  
445 in four BB inventories, and investigate in detail the key reasons for the differences in emission  
446 inventories.

### 3.1 The contribution of dry matter and emission factors to the difference in CO emission

The total global CO emissions from the four BB emission inventories selected for this study are in the range of 252-336 Tg, with GFED4s being the highest and FINN1.5 the lowest. In order to quantify the differences in CO emissions among four datasets, we use the standard deviation (SD) to characterize the absolute difference, and the coefficient of variation (cv, calculated as the ratio of SD to the mean) to characterize the relative differences (Fig. 2a). The larger the cv, the greater the difference between emission inventories. We have ranked the major seven BB regions in the world according to the differences in CO emissions between the four sets of inventories, with the differences being, in descending order, EQAS, BONA, SEAS, SHAF, NHAf, BOAS, and SHSA.

This study points to a high variability of different BB emission inventories in EQAS, which is inconsistent with previous studies (Liu et al., 2020b; Pan et al., 2020). Previous studies mainly focused on emission differences of particulate pollutants, such as BC and OC (Bian et al., 2007; Paton-Walsh et al., 2012; Carter et al., 2020; Lin et al., 2020b; Pan et al., 2020), thus assuming that the inventory differences in Equatorial Asia are smaller than those in Southern Hemispheric Africa and Northern Hemispheric Africa. In contrast, this study analyzes the differences between particulate and gaseous pollutant emissions separately when comparing the differences in BB emission inventories. For example, GFED4s classify a large portion of EQAS land cover as peatland (Kasischke and Bruhwiler, 2002; Stockwell et al., 2016; van der Werf et al., 2006, 2010a, 2010b, 2017) and suggest that this organic matter-rich soil emits a large amount of CO when burned. The other three inventories either do not include peatland (FINN1.5 and QFED2.5) or only consider peatlands as a small fraction of the burned area in EQAS (VFEI0), thus estimating CO emissions much smaller than GFED4s. In addition, the extent of peatland fires in EQAS increased significantly during the strong El Niño event (Page et al., 2002). Considering that a strong El Niño event also occurred in 2015-2016, these increases in peatland fires further amplify the discrepancy between GFED4s and other emission inventories on CO estimates.

~~According to Eq. (1), we split the difference in CO emission into the difference in EFs and DM (Fig. 2b and c). Since only GFED4s provides DM information in its dataset, we follow Carter (2020) to divide CO emissions per grid by the EF applied to each biome to obtain DM:~~

$$DM_{b,x} = CO_{b,x} / EF_b \quad (6)$$

~~where b represents one of the seven biomes in Fig. S1, and x represents the location grid. The calculation of DM by CO is somewhat representative, since all inventories are not corrected for CO emission factors. After calculating the  $DM_{b,x}$  for each grid, we obtained a regional average emission factor by dividing the total CO emissions by the total DM for each major BB region:~~

$$EF_{LU} = \sum_{b,x} CO / \sum_{b,x} DM \quad (7)$$

~~Such calculations allow us to distinguish the impact of LULC classification on BB emission inventories.~~

As shown in Fig. 2, the distribution pattern of DM differences is very similar to that of CO emission differences, indicating that DM is the main reason for dominating the difference in the four emission inventories. In comparison, the difference in DM contributes 50-80% to the regional CO emission differences, and the comprehensive EFs contributes the remaining 20-50%. However, in EQAS, BONA, and BOAS, the contribution of comprehensive EFs to BB emission differences in four datasets is comparable to that of DM (Fig. 2). In the following sections, we will further analyze the main causes of the differences for DM and EFs.

## 491 3.2 Primary causes of DM inconsistency in the bottom-up inventories

492 To investigate the underlying causes of the differences in DM, we first compared DM between  
493 emission inventories produced by the bottom-up and up-down approaches. The difference in DM  
494 estimated by the top-down method is small, and the DM ratio of QFED2.5 to VFEI0 does not exceed  
495 two times in different regions. However, DM estimated by the bottom-up approach varied widely,  
496 with DM ratio as high as 4.7 in BONA for GFED4s and FINN1.5 during the 2013-2016 fire season.  
497 Therefore, we need to focus on the main reasons for DM variance in emission inventories based on  
498 bottom-up approach.

499 According to Eq. (2), DM equals the product of the burned area, fuel load, and FB in the bottom-  
500 up inventories, with the product of the last two terms being fuel consumption. Fig. 3 compares the  
501 burned area and fuel consumption of GFED4s and FINN1.5 emission inventories for the seven  
502 largest BB regions. The ratio GFED4s/FINN1.5 represents the relative difference in burned area or  
503 fuel consumption between the two emission inventories. In general, the difference in burned area  
504 between the two inventories varies greatly with latitude, and the ratio of GFED4s to FINN1.5  
505 fluctuates in the range of 0.28-1.94. In contrast, differences in fuel consumption between the two  
506 inventories were more consistent, with GFED4s consistently having higher fuel consumption than  
507 FINN1.5 in all regions except SEAS. In the next sections, we discuss the main reasons for the  
508 differences in burned area and fuel consumption between the two datasets.

### 509 3.2.1 Effect of land cover on burned area

510 As shown in Fig. 3a, the differences in the burned area between the bottom-up emission  
511 inventories ~~is-are~~ highly variable. At high latitudes, the burned area of GFED4s is significantly  
512 higher than that of FINN1.5, especially in BONA, where the burned area of GFED4s is twice that  
513 of FINN1.5. In contrast, the burned area of GFED4s in the equatorial region is much lower than that  
514 of FINN1.5, and even 60% smaller in EQAS. This is a result of the difference in fire detection  
515 between the two datasets. As shown in Table 1, FINN1.5 uses the MCD14 DL fire point product,  
516 while GFED4s uses the hybrid burned area product, mainly using MCD64A1 combined with fire  
517 point products MOD14A1/MYD14A1 to enhance the detection of small fires.

518 These two sets of products have their ~~own~~ advantages in detection ability under different  
519 vegetation type conditions. The hybrid burned area product detects burned areas over a period of  
520 time (up to days), while the fire point product detects burned areas primarily in near ~~real-real~~-time  
521 (Roy et al., 2008). In addition, the burned area used in GFED4s (hybrid burned area product) is not  
522 affected by the vegetation canopy when the leaf area index (LAI) is less than 5. Therefore, a higher  
523 burned area is estimated in GFED4s in BONA and BOAS than in FINN1.5. However, in areas with  
524 more broadleaf forests and grasslands such as EQAS, SEAS, and SHSA (Fig. S2), the MCD14DL  
525 fire point product used in FINN1.5 performed better in capturing understory fires that occurred in  
526 closed canopies (Cochrane and Laurance, 2002; Cochrane, 2003; Alencar et al., 2005; Roy et al.,  
527 2008). It also has an advantage in capturing sporadic and fragmented small fires in grasslands and  
528 agricultural fields due to its high resolution (Liu et al., 2020b). Furthermore, FINN1.5 assumes that  
529 each detected fire in the equatorial region will continue to burn for 2 days, and that the next day's  
530 fire will continue to be half the size of the previous day (Table 1). Thus, the burned area of FINN1.5  
531 in the tropical zone is 2.6 times higher than ~~those-that~~ of GFED4s, which is consistent with previous  
532 studies (Wiedinmyer et al., 2011; Pan et al., 2020). At the equator, the burned area in

533 grassland/agricultural fields and forests estimated by FINN1.5 is 1-3 and 4-6 times higher than in  
534 GFED4s, respectively (not shown).

535 It is worth noting that in Africa (NHAf and SHAF), although the dominant burnable vegetation  
536 is grassland (Fig. S2), unlike the sporadic small fires that occur in grassland in the other five regions,  
537 large continuous fires often occur in African Savannas (Liu et al., 2020b). Therefore, the hybrid  
538 burned area product used in GFED4s is more effective in detecting all fire events occurring over a  
539 ~~period-of-time~~, with 10-20% higher burned area than FINN1.5.

### 540 3.2.2 Effect of cloud obscuration on burned area

541 In addition to the vegetation, cloud occlusion can likewise bias the satellite detection of burned  
542 area. Figure S3 shows the time series of AOD measured by satellite or ground-based data at the  
543 Pickle Lack site of BONA from June to August 2013. In contrast to the high AOD values observed  
544 for the AERONET network, MODIS AOD ~~is~~ often in missing measurements when the MODIS  
545 cloud fraction is larger than 0.5. Furthermore, AERONET AOD varies dramatically over a short  
546 ~~period-of-time~~, suggesting that different detection principles (such as detecting fire points in near  
547 real-time during satellite overpass time, or estimating the accumulation of burned area over time  
548 through changes in surface albedo over multiple satellite overpass times) can significantly affect the  
549 burned area product under high cloud fraction/smoke conditions (Paton-Walsh et al., 2012; Liu et  
550 al., 2020b; Pan et al., 2020). Although some assumptions are made in FINN1.5 in the equatorial  
551 regions as described above to improve the effect of cloud obscuration on burned area detection,  
552 these assumptions are not used for mid- and high-latitudes. GFED4s uses a hybrid burned area  
553 product and is relatively unaffected by cloud obscuration. By fusing the MCD64A1 with  
554 MOD14A1/MYD14A1 products with multi-temporal satellite data, GFED4s is able to determine  
555 the approximate date and extent of fires through post-fire ash deposition, vegetation migration, and  
556 land surface changes (van der Werf et al., 2017; Boschetti et al., 2015, 2019).

557 To quantitatively assess the impact of cloud obscuration on different emission inventory estimates,  
558 we perform ~~analyzes-analyses~~ in areas with high cloud fraction (Fig. S4), intense biomass burning,  
559 and unaffected by the smoothing hypothesis used in FINN1.5. We selected the regions of North  
560 America with the most intense biomass burning (Alberta and Saskatchewan, Canada, 50°-70°E,  
561 100°-130°W, Fig. S5), and analyzed the relationship between the burned area and cloud fraction for  
562 bottom-up inventories during July from 2013 to 2016 (Fig. S6). As shown in Fig. 4, with the increase  
563 in cloud fraction, ~~the~~ SMAPE of the two bottom-up emission inventories increases from 150% to  
564 180%, while the Pearson correlation declines from 0.85 to around 0.75. These results demonstrate  
565 that the uncertainty in the burned area for two bottom-up emission inventories increases by ~20%  
566 during high cloud fraction compared to low cloud fraction conditions.

### 567 3.2.3 Causes of Fuel Consumption differences

568 Fuel consumption is another factor that affects DM differences between two BB emission  
569 inventories. As shown in Fig. 3b, the fuel consumption of GFED4s is 30-75% higher than that of  
570 FINN1.5 in almost all BB areas except SEAS. The difference in fuel consumption between the two  
571 emission inventories is larger in the tropics than in the high latitudes. ~~In this study, we invert the~~  
572 ~~fuel consumption for each vegetation biome b in a given area as follows:~~

$$573 \text{-----} FC_b = DM_b/BA \text{-----} (8)$$

574 ~~The DM corresponding to each biome in FINN1.5 and GFED4s has been obtained according to~~  
575 ~~equation (6), and BA is the total burned area obtained from the emission inventory.~~ As shown in Fig.  
576 5, at high latitudes (e.g., BONA and BOAS), and in the equatorial region (such as EQAS), relatively  
577 high fuel consumption comes from peatlands in GFED4s. According to previous studies, peatlands,  
578 a type of soil rich in organic matter, store large amounts of carbon underground (van der Werf et al.,  
579 2010b, 2017; Gibson et al., 2018; Kiely et al., 2021; Vetrina et al., 2021), and emit large amounts of  
580 CO when burned. Peatlands contribute 30-60% of the total fuel consumption in BONA, BOAS, and  
581 EQAS (Fig. 5a-c).

582 Besides peatlands, GFED4s tends to have higher fuel consumption than FINN1.5 due to forest  
583 contributions. Forests (including tropical, temperate, and boreal forests) account for more than 50%  
584 of the fuel consumption in all burning regions except EQAS, where peatlands dominate the fuel  
585 consumption. Moreover, forest fuel consumption in GFED4s is generally much higher than in  
586 FINN1.5 except in BOAS and SEAS (Fig. 5). Since fuel consumption is equal to the product of fuel  
587 load and FB (the percentage of specific plants that can be adequately burned, Eq. 2), different  
588 vegetation classifications may be responsible for large differences in fuel consumption between  
589 emission inventories. For example, for woody vegetation such as forests, GFED4s assumes a range  
590 of FB between 40-60% for temperate and tropical forests and 20-40% for boreal forests, while  
591 FINN1.5 assumes that all woody vegetation burns no more than 30% (van der Werf et al., 2010;  
592 Wiedinmyer et al., 2011). Thus, in terms of FB alone, the forest fuel consumption of GFED4s is  
593 therefore 0.67-1.3 times greater than that of FINN1.5, which is one of the main reasons for the  
594 difference in fuel consumption.

### 595 3.3 Primary causes of DM inconsistency in the top-down approach

596 We also analyze the causes of the difference in DM between BB emission inventories estimated  
597 by the top-down method. According to Eq. (3), it is evident that the empirical factor and the radiative  
598 energy of the fire are the key factors that cause the discrepancy in the top-down emission inventories.  
599 The QFED2.5 and VFEI0 inventories we have chosen use different satellites for the fire detection  
600 products. For example, for the fire radiative power product, QFED2.5 is based on the Moderate  
601 Resolution Imaging Spectroradiometer (MODIS) inversion of the NASA Terra and Aqua combined  
602 satellites, while VFEI0 is based on the Visible Infrared Imaging Radiometer (VIIRS) inversion of  
603 the combined ~~polar-polar~~-orbiting satellites Suomi NPP and NOAA-20, although the algorithms are  
604 similar. However, there are systematic deviations due to different satellites, specific tests and  
605 metadata, and resolutions. The VIIRS 375 m fire product used by VFEI0 has a finer resolution and  
606 is more advantageous for small fire spot detection than other coarser resolution (1 km) fire spot  
607 detection products. The FRP density used in VFEI0 is much higher than that of QFED2.5 due to the  
608 fine horizontal resolution.

609 The estimations of FRP and DM are ~~highly dependent on~~strongly influenced by the horizontal  
610 resolution of satellite products. For example, in the BONA region during July (the month with the  
611 most intense burning at the position of 50°-70°N, 100°-130°W), the total QFED FRP (average FRP  
612 measured by MOD and MYD) is 1.5 times higher than VFEI0 (Fig. S7), ~~).~~ Additionally, the differing  
613  $\alpha$  values between QFED2.5 and VFEI0 in BONA can potentially result in higher DM in QFED2.5  
614 compared to VFEI0 by a factor of 1.3-3.8. However, the actual ~~but~~ DM in the QFED2.5 inventory  
615 is 30% lower than in VFEI0. The relatively high FRP density used in VFEI0 (Fig. S8) results in a  
616 higher DM than in QFED2.5 due to its ~~higher-superior~~ horizontal resolution, enabling which



~~facilitates capturing the~~ precise ~~areas delineation~~ of fire ~~areas~~. ~~It is important to n~~Note that ~~while~~ the empirical factor also ~~has an impact influences on~~ the amount of DM, ~~but its impact~~ should not be as significant as the difference caused by the horizontal resolution of satellite products (Kaiser et al., 2012; Darmenov et al., 2015; Ferrada et al. 2022).

Previous studies have shown that cloud occlusion also causes bias in FRP detection (Liu et al., 2020b). We also take BONA as a pilot region to analyze the influence of cloud fraction on FRP in QFED2.5 and VFEI0. According to Fig. 5c-d, the SMAPE of the two emission inventories rises as the cloud fraction increases, and ~~the~~ Pearson correlation is noticeably low under the maximum cloud fraction. While QFED2.5 uses the "sequential approach" (section 2.1) to correct for the missing FRP in cloud-obscured fires, this correction is not considered in VFEI0. Therefore, although the two top-down emission inventories use similar algorithms, significant bias occurs under high cloud fraction conditions, with QFED2.5 estimating DM much higher than VFEI0.

### 3.4 Primary causes of EF inconsistencies

Although DM differences dominate the inconsistencies of CO emissions across major BB regions, the contribution of EFs is still not negligible in some regions. For example, in EQAS, BONA, and BOAS, the contribution of EFs is up to 50%, which is comparable to that of DM. ~~Considering that EF is closely related to vegetation types, we calculated the emission factor of a single biome type in a given region as follows:~~

$$EF_b = CO_b / \sum_b DM \quad (8)$$

~~where b represents one of the seven biome classifications in this study (Fig. S1), and DM here is the sum of the value from each biome in a certain region.~~

—The comprehensive EFs of GFED4s are higher in BONA, BOAS, and EQAS regions than in other inventories, with vegetation classification being one of the most important factors (Fig. 6). For example, in EQAS at low latitudes, peatlands in GFED4s account for 65% of the regional comprehensive EF. In contrast to GFED4s, FINN1.5, and QFED2.5 do not consider this organic matter-rich land as a source of burning, and they classify this category of land cover type as savanna or grass. The CO emission factor for peatlands is four times higher than the CO emission factor for savanna or grass (Table 2), ultimately making the comprehensive EF for GFED4s 60-70% higher than that of the other three datasets. It is worth noting that although the classification of Peatland exists in VFEI0 (Ferrada et al., 2022), due to differences in terrestrial ecological divisions (Olson et al., 2001; <http://www.worldwildlife.org/science/data/item1875.html>), peatlands identification areas are much smaller than GFED4s inventory. Therefore CO emissions from peatlands in GFED4s are much higher than in the VFEI0 inventory (Figure 3-9a; Ferrada et al., 2022).

In both BONA and BOAS, we find that the comprehensive EFs in the four datasets are ranked as follows: GFED4s>FINN1.5>QFED2.5>VFEI0, where the EF of GFED4s is about 1.5 times higher than that of VFEI0. Unlike the low-latitude regions, the classification of forests in different emission inventories is the main reason for the difference in comprehensive EF in high-latitude regions. At high latitudes (50° - 70°N), GFED4s, QFED2.5, and FINN1.5 identify more forests than VFEI0 (Fig. S1) because the former three classify some shrubs (e.g., closed shrublands and woody savanna) as forests, while the latter classify them as grassland. Forests contribute to 70% ~~and or~~ more of the comprehensive EFs at high latitudes in the first three emission inventories, but only 8% to the comprehensive EF in VFEI0. The remaining gap in the absolute contribution of forests is caused by the difference in the selected emission factors and the horizontal resolution of the satellite products.

### 660 3.5 Contribution of DM and EFs to differences in OC emissions

661 The above analysis completes the comparison of gaseous pollutant CO among different emission  
662 inventories. In this section, we will take OC as an example to compare the emission differences of  
663 particulate pollutants. As shown in Fig. 7, the global OC emissions of four datasets range from 14.9  
664 to 42.9Tg, with the highest emissions from QFED2.5, which is consistent with previous studies  
665 (Carter et al., 2020; Pan et al., 2020). According to the statistical method in section 3.1, we  
666 quantified the magnitude of OC emission differences between regions and ranked them as follows:  
667 BONA>BOAS>NHAF>SHAF>SEAS>SHSA>EQAS. Compared to the CO emission differences  
668 (Fig. 2), the difference in OC emissions becomes larger for BOAS and smaller for low latitude  
669 regions of SEAS and EQAS. Since DM should be consistent in the same emission inventories for a  
670 given time and area, the magnitude of emissions for different species depends on changes in  
671 emission factors. Considering that the emission factors of aerosol-related emission species such as  
672 OC, BC, NH<sub>3</sub>, SO<sub>2</sub>, and PM<sub>2.5</sub> have been corrected based on the satellite retrieved AOD of the  
673 QFED2.5 emission inventory (Table 2), the EFs of OC in QFED2.5 are much higher than that of the  
674 other three emission inventories (Fig. 7b). As a result, the OC EFs in the QFED2.5 emission  
675 inventory were enlarged by a factor of 1.8-4.5 times through the correction of BOAS, SEAS and  
676 EQAS (Table 2). In contrast, the other three emission inventories were not corrected for OC EFs.

677 Unlike the CO EFs, the OC EFs of GFED4s in equatorial regions are largely consistent with the  
678 FINN1.5 and VFEI0 emission inventories. Although burning organic matter-rich soil substrates is  
679 generally thought to release large amounts of CO, their ability to release OC is similar to that of  
680 vegetation such as shrubs and some forests. Thus, despite CO emissions bias in EQAS being  
681 largely affected by peatlands, differences in OC emissions among the four inventories are not  
682 significant.

683 Compared with Pan et al. (2020), it is obvious that the top-down approach will not lead to an  
684 increase in emission deviation of the particulate-phase species. The correction of EFs, however, is  
685 the root cause of the increased bias in OC emissions. Pan et al. (2020) reported that QFED2.5 and  
686 FEER1.0 had the highest global OC emissions, while GFAS1.2 had much lower OC emissions. In  
687 this study, the largest OC emission also appears in QFED2.5, but the global total OC emissions of  
688 the recently released VFEI0 are relatively low.

## 689 4 Model evaluation based on emission inventories application

### 690 4.1 Comparison of simulations with MOPITT CO

691 One of the main goals of this study is to provide a confidence assessment of the BB emission  
692 inventories by comparing model simulations with observations. A comparison between model  
693 simulations using different emission inventories and ground-based/~~satellite-satellite~~-retrieved data  
694 for the respective fire seasons (Table 3) of the main BB regions is explored below. In this study, we  
695 compared the model results with measurements from two perspectives: the spatial distribution of  
696 BB pollutants, and the time-varying characteristics of BB pollutants.

697 Figure 8 depicts the spatial distribution of CO column burdens in SHSA and SHAF during the  
698 fire seasons. In SHSA, the simulated CO column burdens using different emission inventories are  
699 all consistent with the spatial distribution pattern of MOPITT CO column burden, with the peak  
700 value located in the Amazon rainforest. However, the central value of MOPITT CO column burden

701 is as high as  $2.8 \times 10^{18}$  molecules  $\text{cm}^{-2}$ , which is slightly higher than the simulated results. Among  
702 the four sets of emission inventories, the peak amplitude and spatial distribution of simulated CO  
703 column burdens are closest to the ~~satellite-satellite~~-retrieved data after applying the GFED4s and  
704 VFEI0. In SHAF, however, the model underestimated the peak CO column burden after applying  
705 all emission inventories except VFEI0.

706 In addition to SHSA and SHAF, a comparison of regionally averaged CO column burdens  
707 between our simulations and MOPITT CO in major BB regions is also shown in Table 3. In the  
708 Northern Hemisphere, our simulations are significantly underestimated compared to MOPITT CO,  
709 while those in the Southern Hemisphere are consistent with satellite retrievals. Surprisingly, the  
710 simulated spatial distributions and magnitudes of CO in the Southern Hemisphere using the recently  
711 released VFEI0 agree very well with observations. In contrast, the underestimation of CO  
712 concentrations in the Northern Hemisphere is partly due to uncertainty in anthropogenic emissions,  
713 as we assume anthropogenic emissions at 2010 levels, which are lower than those during the 2013-  
714 2016 period.

715 Note that simulated CO concentrations are 30-40% lower than MOPITT CO at high latitudes.  
716 Besides the impact of emission inventories, there are also large uncertainties in satellite-retrieved  
717 CO concentrations (Lin et al., 2020a; Pan et al., 2020). In addition, OH loss, long-range transport,  
718 and photochemical reactions involved in the CESM2-CAM6 model simulations also lead to  
719 uncertainties in simulated CO. For example, MOZART-4x contains an additional OH oxidation  
720 pathway for CO, which may lead to lower CO concentrations (Lamarque et al., 2012; He and Zhang,  
721 2014; Barré et al., 2015; Brown-Steiner et al., 2018; Emmons et al., 2020). In comparison, the  
722 simulated CO by using GFED4s is closest to the MOPITT CO value in terms of spatial distribution  
723 and peak magnitude at high latitudes in ~~the~~ Northern Hemisphere, which is superior to other  
724 emission inventories.

## 725 **4.2 Comparison of simulations with MODIS AOD**

726 We compared MODIS-derived aerosol optical depth (AOD) data with simulated AOD in major  
727 BB areas. Figure 9 shows the spatial distribution of AOD in SHSA and SHAF during their fire  
728 seasons. The simulated AOD is significantly higher than the MODIS AOD in SHSA. Note that  
729 primary organic aerosols (POA) associated with BB account for only 15-23% of the total AOD in  
730 Amazon, while secondary organic aerosols (SOA) account for approximately 50% of the total AOD.  
731 Furthermore, overestimation of simulated AOD occurs throughout the year, not just during the fire  
732 season. Considering the high biogenic emissions in this region, the overestimation of AOD could  
733 be attributed to the formation of biogenic SOA (He et al., 2015; Tilmes et al., 2019). In SHAF, the  
734 spatial distribution and magnitude of simulated AOD using GFED4s and VFEI0 are close to those  
735 of the MODIS AOD. In comparison, our results show that AOD is significantly underestimated  
736 using FINN1.5, but largely overestimated using QFED2.5.

737 Table 4 shows the mean values of model-simulated AOD and satellite measurements for each  
738 region during its fire season. The influence of the BB emission inventory has little effect on the  
739 simulated AOD value in the Southern Hemisphere, and the regional average AOD deviation is  
740 within 20%. In contrast, the average deviation of simulated AOD driven by four BB inventories can  
741 be as high as 40% in the high latitudes of the Northern Hemisphere. Comparatively, GFED4s and  
742 QFED2.5 are more suited for high latitudes in the northern hemisphere, whereas the VFEI0 is most

743 suitable for the southern hemisphere for AOD simulations. In Africa, QFED2.5 is not recommended  
744 due to its considerable overestimation.

### 745 4.3 Comparison of simulations with ground-based measurements

746 In the above sections, we merely discussed the spatial distribution and the magnitude of pollutants  
747 during fire seasons. To further analyze whether each dataset can effectively capture the  
748 instantaneous combustion of BB, we compared the value of simulated daily AOD with that of  
749 ground-based observation (Fig. 10). ~~In order to~~ To be more representative, we selected stations in  
750 each BB region with a large amount of data during fire season, allowing a comprehensive  
751 assessment of the global BB emission inventories. The specific locations of the selected 12  
752 AERONET sites are shown as red triangles in Fig. 1b.

753 At EQAS sites such as Palangkaraya and Jambi, the observed AOD from September to November  
754 ~~in~~ 2014/2015 is generally higher than 1, with peaks exceeding 5, reflecting the intense BB events  
755 (Fig. 10a-b). Only simulations using GFED4s are consistent with observed AOD during strong BB  
756 events, with a slight underestimation of 33-38%, while none of the other simulations could capture  
757 the BB process. Considering the significant contribution of peatlands to BB emissions in EQAS in  
758 GFED4s, our results suggest that it is important to include the burning of organic matter-rich soils  
759 in BB emission inventories. At SEAS sites such as Omkoi and Ubon Ratchathani, the peak AOD  
760 occurs from February to April at a value of about 2, and all simulations applying the four emission  
761 inventories capture the observed changes in AOD (Fig 10c-d). However, due to the uncertainty of  
762 anthropogenic emissions, the simulated AOD is usually smaller than the actual observed value in  
763 EQAS. Note that simulations using QFED2.5 are most consistent with observed AOD during intense  
764 biomass burning events.

765 At the Namibe station of SHAF (Fig. 10e), the simulated AOD agrees best with the measured  
766 results after using FINN1.5 and GFED2.5, with NMB values within  $\pm 8\%$ , indicating these two  
767 emission inventories can characterize the day-to-day variability of the intense BB process. However,  
768 Namibe is located downwind of the dust source, and dust aerosols contribute more than 50% to the  
769 total AOD in this area. To better evaluate the performance of the four BB emission inventories in  
770 SHAF, we chose another site, Mongu Inn, located in the interior of Southern Hemispheric Africa,  
771 where dust and sea salt accounted for 20-30% of the total AOD. At Mongu Inn, all simulations  
772 underestimate AOD by 46-71%, and only QFED2.5 and VFEI0 emission inventories ~~are able to can~~  
773 capture a few peaks during intense biomass burning events (Fig. 10f). In SHSA, while Figures 9  
774 and 10h show an overall overestimation of simulated AOD compared to MODIS AOD, at the  
775 Brazilian Alta Floresta site east of the Amazon, simulated AOD agrees very well with the ground-  
776 based observations (Fig. 10g). In general, the simulations using the VFEI0 emission inventory for  
777 the Southern Hemisphere are close to the measurements.

778 At high latitudes, simulations driven by GFED4s and QFED2.5 better capture the observed peak  
779 AOD, with regional NMB values of less than 40% (Fig. 10i-l), suggesting that these two simulations  
780 can reproduce the intense BB process. In contrast, FINN1.5 and VFEI0 are obviously not suitable  
781 for describing the BB process in these sites, and the simulated AOD is underestimated by 60-80%.

## 782 5 Conclusion and Discussion

783 ~~The establishment of BB emission inventories follows two basic approaches, one is a "bottom-~~

784 up” approach, which usually establishes inventory information based on observed surface data (such  
785 as detected fire points, burned area, and vegetation types). The other one is a “top-down” approach,  
786 that is, the vegetation consumption is inversely calculated from the radiative energy release rate of  
787 vegetation burning observed by satellite, and the vegetation type information is superimposed to  
788 establish the inventory. In this study, we examine four commonly used BB emission inventories  
789 (two bottom-up inventories (GFED4s and FINN1.5) and two top-down inventories (QFED2.5 and  
790 VFEI0)) are chosen to better understand the uncertainty uncertainties of associated with BB  
791 emissions, two of which are bottom up inventories (GFED4s and FINN1.5), and two are top-down  
792 inventories (QFED2.5 and VFEI0). We analyze the difference variations in CO and OC emissions  
793 across from these inventories for seven major BB regions around the world worldwide from 2013  
794 to 2016. We explore the differences between gaseous and particulate emission inventories, and  
795 quantify the impact of vegetation classification, cloud cover, and emission factors on emission  
796 inventory bias. Additionally, we also applied the four these BB emission inventories to the global  
797 model CESM2-CAM6 to assess the model’s ability performance to in simulating pollutants, by  
798 comparing the simulations with measurements from against satellite products or and ground-based  
799 observations.

800 The total global CO emissions exhibit significant variability in among the four inventories vary  
801 greatly, with their annual average values fluctuating ranging between from 252- to 336 Tg, and the  
802 a maximum deviation rate exceeds 30%. In some certain regions such as BONAs, changes in  
803 CO emissions are even larger. For example, GFED4s in BONA emits 5.8 times more CO emissions  
804 than FINN1.5, while the coefficient variation of the four emission inventories in EQAS is as high  
805 as 0.67. Overall, CO emissions from GFED4s are higher than those from VFEI0 and QFED2.5  
806 inventories in all regions, with the lowest CO emissions in FINN1.5 inventory. DM is dominates  
807 identified as the primary contributor to the variance among BB emission inventories, accounting for  
808 50-80% of the regional bias, while comprehensive EFs account for contribute the remaining 20-50%.  
809 Notably Interestingly, the contributions of DM and comprehensive EFs to the emission inventory  
810 differences in BB emission inventories are comparable across equatorial regions and Northern  
811 Hemisphere high latitudes.

812 There is a large uncertainty in DM due to arises from the calculation of underlying fuel  
813 consumption and burned area, which in turn is related linked to the vegetation classification method,  
814 fire detection product algorithm, and cloud/smoke masking used in the emission inventory. First,  
815 the V vegetation classification method significantly impacts affects fuel loading and the Fraction of  
816 Biomass burned, with discrepancies contributing to biases in fuel consumption. At In regions at  
817 both low and high latitudes (except Southeast Asia), the fuel consumption term of FINN1.5 is  
818 exhibits a fuel consumption term that is less than 50% of that of GFED4s, where with the  
819 vegetation classification method ology contributes contributing significantly primarily to this bias.  
820 For example, in EQAS, while GFED4s classifies a significant portion of the area as peatland,  
821 FINN1.5 identifies it as grassland, resulting in 37% lower fuel consumption for FINN1.5 than  
822 GFED4s in this region. In addition, GFED4s assumes that the FB of tropical forest is 40-60%, while  
823 FINN1.5 assumes that the FB of forests does not exceed 30%, so the FB of forests in FINN1.5 is  
824 25-50% lower than GFED4s. Similarly, the fuel consumption of FINN1.5 in high latitudes is also  
825 lower than that of GFED4s, with a deviation of up to 50% or more. The classification of peatlands,  
826 the amount of forest burnable (fuel load) and burning percentage of the forest remain the main  
827 contributions. Second, different fire detection products can also cause introduce bias in the

828 estimated burned area, ~~leading to affecting~~ uncertainty in DM. ~~For example, the MCD14DL used in~~  
829 ~~FINN1.5 identifies fire points based on brightness temperature, which can effectively detect~~  
830 ~~understory burns in tropical rainforests, and can easily capture small area burns in agricultural fields.~~  
831 ~~Furthermore, combined with the smoothing assumptions for equatorial regions, the estimated~~  
832 ~~burned area in FINN1.5 is generally larger than that in GFED4s at low latitudes. Last but not least,~~  
833 ~~s~~~~Satellite transit/cloud obscuration can similarly affect/influences~~ DM ~~between emission inventories~~  
834 ~~by influenceing-affecting the burned area/fire radiative energy/identification of burned area/fire~~  
835 ~~radiative energy. In the Africa grasslands where fires develop rapidly, due to the fast fuel~~  
836 ~~consumption, the burned area often has a large difference in a short period of time. If the fire point~~  
837 ~~monitoring product based on brightness temperature data identification is used, there may be missed~~  
838 ~~detections of fire that occur during the satellite transit/cloud occlusion, but fire area product~~  
839 ~~identified based on surface albedo changes can better avoid missed detections caused by satellite~~  
840 ~~transit/cloud occlusion. Cloud cover at high latitudes substantially has a significant impacts on the~~  
841 ~~uncertainty of emission inventories uncertainty-, with~~ According to our results, the bias between  
842 ~~bottom-up (or top-down) emission inventories in BONA increased~~ by 20% in July in BONA with  
843 ~~under increased-higher~~ cloud fraction.

844 ~~We extend our analysis to~~ In addition to gaseous emissions, we also analyzed the differences in  
845 ~~emissions of~~ particulate pollutants, ~~among emission inventories using OC emissions as an example.~~  
846 ~~The four sets of BB emission inventories fluctuate between 14.9 and 42.9 Tg of g~~Global average  
847 ~~annual OC emissions vary widely among the four inventories, ranging from 14.9 to 42.9 Tg, a~~  
848 ~~greater variation than the gaseous species demonstrating greater variability than gaseous species like~~  
849 ~~CO. Similar to the results for CO emission variability, current BB emission inventories have large~~  
850 ~~variability at high northern latitudes. Unlike differences in CO emissions, there is less variability in~~  
851 ~~comprehensive EFs over the equator. In particular, the QFED2.5 inventory adjusted emission factors~~  
852 ~~using satellite aerosol optical thickness (AOD) to enhance emissions of particulate matter including~~  
853 ~~OC. In addition, peatlands only have comparable OC emission capacity to the shrub, which makes~~  
854 ~~the impact of vegetation classification differences on OC EFs less significant, ultimately resulting~~  
855 ~~in lower variability in particle phase emissions in equatorial regions. BB OC emissions exhibit large~~  
856 ~~variability at high latitudes in the Northern Hemisphere, with QFED2.5 adjusting emission factors~~  
857 ~~based on satellite aerosol optical thickness (AOD) to enhance particulate matter emissions.~~

858 ~~We a~~Applying ~~ied~~ four sets of BB emission inventories to CESM2-CAM6, ~~and we~~ compared ~~the~~  
859 ~~model-simulated CO column concentrations with the MOPITT satellite inversion CO column~~  
860 ~~concentrations. According to our simulations, CO simulated using GFED4s is closest to satellite~~  
861 ~~observations in almost all regions except southern Asia and Africa. We also compared model results~~  
862 ~~with AOD retrieved from MODIS satellites or measured by AERONET. Simulated AOD at high~~  
863 ~~northern latitudes is often underestimated when using current mainstream BB emission inventories.~~  
864 ~~For example, the simulated regional average AOD is 8-46% lower than MODIS in North America.~~  
865 ~~Unlike the high latitudes, the simulated AOD is significantly overestimated at the equator, and the~~  
866 ~~regional average AOD simulated by the model in Northern Hemispheric Africa is 66-91% higher~~  
867 ~~than MODIS. In addition, comparing model simulated AOD with AERONET ground-based~~  
868 ~~observations, we find that GFED4s performs best in EQAS for daily variability during intense~~  
869 ~~burning. In SEAS, although FINN1.5 can better represent the magnitude of the overall OC~~  
870 ~~emissions in the BB season, QFED2.5 can capture the day-to-day variation characteristics of intense~~

871 combustion. In the Southern Hemisphere, the latest VFEI0 emission inventory performs well, and  
872 the simulated AOD is able to capture the BB processes.

873 Our study assesses the global applicability of BB emission inventories and has some implications  
874 for future studies. Overall, GFED4s and QFED2.5 inventories for the northern high latitudes  
875 capture the magnitude and daily variation of OC emitted throughout the BB season. These two  
876 emission inventories outperformed the others when applied to studies of interactions between BB  
877 aerosol and weather/climate. In the Southern Hemisphere, the spatial distribution and daily variation  
878 characteristics of CO and AOD simulated by the model are closest to the observed values when the  
879 latest VFEI0 emission inventory is applied. For the equator, the situation is more complicated, and  
880 we recommend combining emission inventories according to the research objectives. For example,  
881 GFED4s performs best in day-to-day changes during intense burning in equatorial Asia. In  
882 Southeast Asia, combining OC magnitude in FINN1.5 and daily variation in QFED2.5 is the optimal  
883 choice.

884 It is worth noting that emission factors (as listed in Table 2) significantly contribute to the  
885 differences in BB emissions. However, actual emission factors vary widely depending on the  
886 different states of combustion (Pokhrel et al., 2021). Further study is needed to understand the  
887 impact of combustion efficiency on the BB EFs and optimize them.

888

889 *Data availability.* The biomass burning emission datasets used in this work are available from  
890 <http://www.globalfiredata.org> (GFED4s), <https://www.acom.ucar.edu/Data/fire/> (FINN1.5),  
891 <https://portal.nccs.nasa.gov/datashare/ies/aerosol/emissions/QFED/v2.5r1/> (QFED2.5), and  
892 <http://bio.cgrer.uiowa.edu/VFEI/DOWNLOAD/> (VFEI0). AOD and cloud fraction from MODIS  
893 dataset can be obtained from <https://ladsweb.modaps.eosdis.nasa.gov/search/>. MOPITT CO can be  
894 obtained from <https://doi.org/10.5067/TERRA/MOPITT/MOP03JM.009>. AERONET AOD is  
895 available from [https://aeronet.gsfc.nasa.gov/new\\_web/download\\_all\\_v3\\_aod.html](https://aeronet.gsfc.nasa.gov/new_web/download_all_v3_aod.html). The Modern-Era  
896 Retrospective analysis for Research and Applications, version 2 (MERRA-2) reanalysis data is  
897 available from <https://gmao.gsfc.nasa.gov/reanalysis/MERRA-2/>. All data analyzed during the  
898 current study are included in this published article and its supplementary information. Raw model  
899 simulations are available from the corresponding author on reasonable request.

900

901

902 *Author contributions.* S. L. and A. D. designed the research, W. H. and S. L. conducted the data  
903 analysis and model simulations, W. H. and S. L. took the lead in writing the manuscript, with  
904 contributions from all authors.

905

906 *Competing interests.* The authors declare that they have no conflict of interest.

907

908 *Acknowledgements.* This work was supported by National Natural Science Foundation of China  
909 (grant number: [42325506](https://doi.org/10.13039/501100011033/20225506), 42075095) and the International Cooperation project of Jiangsu  
910 Provincial Science and Technology Agency (BZ2017066). The numerical modelling was conducted  
911 on computing facilities at the High Performance Computing Centering (HPCC) at Nanjing  
912 University. The authors are grateful to the the AERONET networks for making their data available,  
913 part of the NASA Earth Observing System Data and Information System (EOSDIS). We also thank  
914 the providers of biomass burning emission datasets of GFED, FINN, QFED and VFEI.

915

916

917 **References**

918 Adams, C., McLinden, C. A., Shephard, M. W., Dickson, N., Dammers, E., Chen, J., Makar, P., Cady-  
919 Pereira, K. E., Tam, N., and Kharol, S. K.: Satellite-derived emissions of carbon monoxide, ammonia,  
920 and nitrogen dioxide from the 2016 Horse River wildfire in the Fort McMurray area, *Atmospheric*  
921 *Chemistry and Physics*, 19, 2577-2599, 2019.

922 Akagi, S., Yokelson, R. J., Wiedinmyer, C., Alvarado, M., Reid, J., Karl, T., Crouse, J., and Wennberg,  
923 P.: Emission factors for open and domestic biomass burning for use in atmospheric models, *Atmospheric*  
924 *Chemistry and Physics*, 11, 4039-4072, 2011.

925 Alencar, A., Nepstad, D., and Moutinho, P.: Carbon emissions associated with forest fires in Brazil,  
926 *Tropical deforestation and climate change*, 23, 2005.

927 Alvarado, M., Logan, J., Mao, J., Apel, E., Riemer, D., Blake, D., Cohen, R., Min, K.-E., Perring, A.,  
928 and Browne, E.: Nitrogen oxides and PAN in plumes from boreal fires during ARCTAS-B and their  
929 impact on ozone: an integrated analysis of aircraft and satellite observations, *Atmospheric Chemistry*  
930 *and Physics*, 10, 9739-9760, 2010.

931 Andreae, M. and Rosenfeld, D.: Aerosol–cloud–precipitation interactions. Part 1. The nature and sources  
932 of cloud-active aerosols, *Earth-Science Reviews*, 89, 13-41, 2008.

933 Andreae, M. O.: Emission of trace gases and aerosols from biomass burning—an updated assessment,  
934 *Atmospheric Chemistry and Physics*, 19, 8523-8546, 2019.

935 Andreae, M. O. and Merlet, P.: Emission of trace gases and aerosols from biomass burning, *Global*  
936 *biogeochemical cycles*, 15, 955-966, 2001.

937 Arellano Jr, A. F. and Hess, P. G.: Sensitivity of top - down estimates of CO sources to GCTM transport,  
938 *Geophysical Research Letters*, 33, 2006.

939 Arellano Jr, A. F., Kasibhatla, P. S., Giglio, L., van der Werf, G. R., and Randerson, J. T.: Top - down  
940 estimates of global CO sources using MOPITT measurements, *Geophysical research letters*, 31, 2004.

941 Balshi, M. S., McGuire, A. D., Duffy, P., Flannigan, M., Kicklighter, D. W., and Melillo, J.: Vulnerability  
942 of carbon storage in North American boreal forests to wildfires during the 21st century, *Global change*  
943 *biology*, 15, 1491-1510, 2009.

944 Barré, J., Gaubert, B., Arellano, A. F., Worden, H. M., Edwards, D. P., Deeter, M. N., Anderson, J. L.,  
945 Raeder, K., Collins, N., and Tilmes, S.: Assessing the impacts of assimilating IASI and MOPITT CO  
946 retrievals using CESM - CAM - chem and DART, *Journal of Geophysical Research: Atmospheres*, 120,  
947 10,501-510,529, 2015.

948 Beck, H. E., Zimmermann, N. E., McVicar, T. R., Vergopolan, N., Berg, A., and Wood, E. F.: Present and  
949 future Köppen-Geiger climate classification maps at 1-km resolution, *Scientific data*, 5, 1-12, 2018.

950 Bian, H., Chin, M., Kawa, S., Duncan, B., Arellano, A., and Kasibhatla, P.: Sensitivity of global CO  
951 simulations to uncertainties in biomass burning sources, *Journal of Geophysical Research: Atmospheres*,  
952 112, 2007.

953 Boschetti, L., Roy, D. P., Justice, C. O., and Humber, M. L.: MODIS–Landsat fusion for large area 30 m  
954 burned area mapping, *Remote Sensing of Environment*, 161, 27-42, 2015.

955 Boschetti, L., Roy, D. P., Giglio, L., Huang, H., Zubkova, M., and Humber, M. L.: Global validation of  
956 the collection 6 MODIS burned area product, *Remote sensing of environment*, 235, 111490, 2019.



957 Boucher, O., Randall, D., Artaxo, P., et al.: Clouds and aerosols, *Climate change 2013: The physical*  
958 *science basis, Contribution of working group I to the fifth assessment report of the intergovernmental*  
959 *panel on climate change, Cambridge University Press, 571-657, 2013.*

960 Brando, P. M., Soares-Filho, B., Rodrigues, L., Assunção, A., Morton, D., Tuschneider, D., Fernandes,  
961 E., Macedo, M., Oliveira, U., and Coe, M.: The gathering firestorm in southern Amazonia, *Science*  
962 *Advances*, 6, eaay1632, 2020.

963 Brown-Steiner, B., Selin, N. E., Prinn, R., Tilmes, S., Emmons, L., Lamarque, J.-F., and Cameron-Smith,  
964 P.: Evaluating simplified chemical mechanisms within present-day simulations of the Community Earth  
965 System Model version 1.2 with CAM4 (CESM1. 2 CAM-chem): MOZART-4 vs. Reduced Hydrocarbon  
966 vs. Super-Fast chemistry, *Geoscientific Model Development*, 11, 4155-4174, 2018.

967 Carter, T. S., Heald, C. L., Jimenez, J. L., Campuzano-Jost, P., Kondo, Y., Moteki, N., Schwarz, J. P.,  
968 Wiedinmyer, C., Darmenov, A. S., and da Silva, A. M.: How emissions uncertainty influences the  
969 distribution and radiative impacts of smoke from fires in North America, *Atmospheric Chemistry and*  
970 *Physics*, 20, 2073-2097, 2020.

971 Chen, Y., Li, Q., Randerson, J., Lyons, E., Kahn, R., Nelson, D., and Diner, D.: The sensitivity of CO  
972 and aerosol transport to the temporal and vertical distribution of North American boreal fire emissions,  
973 *Atmospheric Chemistry and Physics*, 9, 6559-6580, 2009.

974 Christian, T. J., Kleiss, B., Yokelson, R. J., Holzinger, R., Crutzen, P. J., Hao, W. M., Saharjo, B. H., and  
975 Ward, D. E.: Comprehensive laboratory measurements of biomass - burning emissions: 1. Emissions  
976 from Indonesian, African, and other fuels, *Journal of Geophysical Research: Atmospheres*, 108(D23),  
977 2003.

978 Christian, K., Wang, J., Ge, C., Peterson, D., Hyer, E., Yorks, J., and McGill, M.: Radiative forcing and  
979 stratospheric warming of pyrocumulonimbus smoke aerosols: First modeling results with multisensor  
980 (EPIC, CALIPSO, and CATS) views from space, *Geophysical Research Letters*, 46, 10061-10071, 2019.

981 Cochrane, M. A.: Fire science for rainforests, *Nature*, 421, 913-919, 2003.

982 Cochrane, M. A. and Laurance, W. F.: Fire as a large-scale edge effect in Amazonian forests, *Journal of*  
983 *Tropical Ecology*, 18, 311-325, 2002.

984 Danabasoglu, G., Lamarque, J. F., Bacmeister, J., Bailey, D., DuVivier, A., Edwards, J., Emmons, L.,  
985 Fasullo, J., Garcia, R., and Gettelman, A.: The community earth system model version 2 (CESM2),  
986 *Journal of Advances in Modeling Earth Systems*, 12, e2019MS001916, 2020.

987 Darmenov, A., da Silvia, A., and Koster, R.: The Quick Fire Emissions Dataset (QFED): Documentation  
988 of Versions 2.1, 2.2 and 2.4. Volume 38; Technical Report Series on Global Modeling and Data  
989 Assimilation, 2015.

990 Deeter, M., Francis, G., Gille, J., Mao, D., Martínez-Alonso, S., Worden, H., Ziskin, D., Drummond, J.,  
991 Commane, R., and Diskin, G.: The MOPITT Version 9 CO product: sampling enhancements and  
992 validation, *Atmospheric Measurement Techniques*, 15, 2325-2344, 2022.

993 Ding, K., Huang, X., Ding, A., Wang, M., Su, H., Kerminen, V.-M., Petäjä, T., Tan, Z., Wang, Z., and  
994 Zhou, D.: Aerosol-boundary-layer-monsoon interactions amplify semi-direct effect of biomass smoke on  
995 low cloud formation in Southeast Asia, *Nature communications*, 12, 1-9, 2021.

996 Duncan, B. N., Martin, R. V., Staudt, A. C., Yevich, R., and Logan, J. A.: Interannual and seasonal  
997 variability of biomass burning emissions constrained by satellite observations, *Journal of Geophysical*  
998 *Research: Atmospheres*, 108, ACH 1-1-ACH 1-22, 2003.

999 Emmons, L.: Coauthors, 2020: The chemistry mechanism in the community earth system model version  
1000 2 (CESM2), *J. Adv. Model. Earth Syst*, 12, e2019MS001882, 2020.

1001 Ferek, R. J., Reid, J. S., Hobbs, P. V., Blake, D. R., and Liousse, C.: Emission factors of hydrocarbons,  
1002 halocarbons, trace gases and particles from biomass burning in Brazil, *Journal of Geophysical Research:*  
1003 *Atmospheres*, 103, 32107-32118, 1998.

1004 Ferrada, G. A., Zhou, M., Wang, J., Lyapustin, A., Wang, Y., Freitas, S. R., and Carmichael, G. R.:  
1005 Introducing the VIIRS-based Fire Emission Inventory version 0 (VFEIv0), *Geoscientific Model*  
1006 *Development*, 15, 8085-8109, 2022.

1007 Firms, L.: Collection 6 NRT hotspot/active fire detections MCD14DL, En ligne: <https://earthdata.nasa.gov/firms> (visité le 21 June 2017), 2017.

1008  
1009 Freitas, S., Longo, K., and Andreae, M.: Impact of including the plume rise of vegetation fires in  
1010 numerical simulations of associated atmospheric pollutants, *Geophysical Research Letters*, 33, 2006.

1011 Freitas, S., Longo, K., Trentmann, J., and Latham, D.: Sensitivity of 1-D smoke plume rise models to the  
1012 inclusion of environmental wind drag, *Atmospheric Chemistry and Physics*, 10, 585-594, 2010.

1013 ~~Friedl, M. A., Sulla-Menashe, D., Tan, B., Schneider, A., Ramankutty, N., Sibley, A., and Huang, X.:~~  
1014 ~~MODIS Collection 5 global land cover: Algorithm refinements and characterization of new datasets,~~  
1015 ~~*Remote sensing of Environment*, 114, 168-182, 2010.~~

1016 GMAO: MERRA - 2 inst3\_3d\_asm\_Np: 3d, 3 - hourly, instantaneous, pressure - level, assimilation,  
1017 assimilated meteorological fields V5. 12.4, 2015.

1018 Gibson, C. M., Chasmer, L. E., Thompson, D. K., Quinton, W. L., Flannigan, M. D., and Olefeldt, D.:  
1019 Wildfire as a major driver of recent permafrost thaw in boreal peatlands, *Nature communications*, 9,  
1020 3041, 2018.

1021 Giglio, L., Randerson, J. T., and van der Werf, G. R.: Analysis of daily, monthly, and annual burned area  
1022 using the fourth - generation global fire emissions database (GFED4), *Journal of Geophysical Research:*  
1023 *Biogeosciences*, 118, 317-328, 2013.

1024 Guenther, A., Jiang, X., Heald, C. L., Sakulyanontvittaya, T., Duhl, T. a., Emmons, L., and Wang, X.:  
1025 The Model of Emissions of Gases and Aerosols from Nature version 2.1 (MEGAN2. 1): an extended and  
1026 updated framework for modeling biogenic emissions, *Geoscientific Model Development*, 5, 1471-1492,  
1027 2012.

1028 He, J. and Zhang, Y.: Improvement and further development in CESM/CAM5: gas-phase chemistry and  
1029 inorganic aerosol treatments, *Atmospheric Chemistry and Physics*, 14, 9171-9200, 2014.

1030 ~~He, J., Zhang, Y., Tilmes, S., Emmons, L., Lamarque, J.-F., Glotfelty, T., Hodzic, A., and Vitt, F.:~~  
1031 ~~CESM/CAM5 improvement and application: comparison and evaluation of updated CB05\_GE and~~  
1032 ~~MOZART-4 gas-phase mechanisms and associated impacts on global air quality and climate,~~  
1033 ~~*Geoscientific Model Development*, 8, 3999-4025, 2015.~~

1034 Hoelzemann, J. J., Schultz, M. G., Brasseur, G. P., Granier, C., and Simon, M.: Global Wildland Fire  
1035 Emission Model (GWEM): Evaluating the use of global area burnt satellite data, *Journal of Geophysical*  
1036 *Research: Atmospheres*, 109, 2004.

1037 Hoesly, R. M., Smith, S. J., Feng, L., Klimont, Z., Janssens-Maenhout, G., Pitkanen, T., Seibert, J. J., Vu,  
1038 L., Andres, R. J., and Bolt, R. M.: Historical (1750–2014) anthropogenic emissions of reactive gases and  
1039 aerosols from the Community Emissions Data System (CEDS), *Geoscientific Model Development*, 11,  
1040 369-408, 2018.

1041 Holben, B. N., Eck, T. F., Slutsker, I. a., Tanre, D., Buis, J., Setzer, A., Vermote, E., Reagan, J. A.,  
1042 Kaufman, Y., and Nakajima, T.: AERONET—A federated instrument network and data archive for  
1043 aerosol characterization, *Remote sensing of environment*, 66, 1-16, 1998.

1044 Huang, X., Ding, K., Liu, J., Wang, Z., Tang, R., Xue, L., Wang, H., Zhang, Q., Tan, Z.-M., Fu, C., Davis,  
1045 S. J., Andreae, M. O., and Ding, A.: Smoke-weather interaction affects extreme wildfires in diverse  
1046 coastal regions, *Science*, 379, 457-461, doi:10.1126/science.add9843, 2023.

1047 Ichoku, C. and Ellison, L.: Global top-down smoke-aerosol emissions estimation using satellite fire  
1048 radiative power measurements, *Atmospheric Chemistry and Physics*, 14, 6643-6667, 2014.

1049 Jiang, Y., Yang, X.-Q., Liu, X., Qian, Y., Zhang, K., Wang, M., Li, F., Wang, Y., and Lu, Z.: Impacts of  
1050 wildfire aerosols on global energy budget and climate: The role of climate feedbacks, *Journal of Climate*,  
1051 33, 3351-3366, 2020.

1052 Junghenn Noyes, K. T., Kahn, R. A., Limbacher, J. A., and Li, Z.: Canadian and Alaskan wildfire smoke  
1053 particle properties, their evolution, and controlling factors, from satellite observations, *Atmospheric  
1054 Chemistry and Physics*, 22, 10267-10290, 2022.

1055 [Kaiser, J., Flemming, J., Schultz, M., Suttie, M., and Wooster, M.: The MACC global fire assimilation  
1056 system: First emission products \(GFASv0\), Tech. Memo. 596, ECMWF, Reading, UK, 2009.](#)

1057 Kaiser, J., Heil, A., Andreae, M., Benedetti, A., Chubarova, N., Jones, L., Morcrette, J.-J., Razinger, M.,  
1058 Schultz, M., and Suttie, M.: Biomass burning emissions estimated with a global fire assimilation system  
1059 based on observed fire radiative power, *Biogeosciences*, 9, 527-554, 2012.

1060 Kasischke, E. S. and Bruhwiler, L. P.: Emissions of carbon dioxide, carbon monoxide, and methane from  
1061 boreal forest fires in 1998, *Journal of Geophysical Research: Atmospheres*, 107, FFR 2-1-FFR 2-14,  
1062 2002.

1063 Kiely, L., Spracklen, D., Arnold, S., Papargyropoulou, E., Conibear, L., Wiedinmyer, C., Knote, C., and  
1064 Adrianto, H.: Assessing costs of Indonesian fires and the benefits of restoring peatland, *Nature  
1065 communications*, 12, 7044, 2021.

1066 Knorr, W., Dentener, F., Hantson, S., Jiang, L., Klimont, Z., and Arneeth, A.: Air quality impacts of  
1067 European wildfire emissions in a changing climate, *Atmospheric Chemistry and Physics*, 16, 5685-5703,  
1068 2016.

1069 Lamarque, J.-F., Emmons, L., Hess, P., Kinnison, D. E., Tilmes, S., Vitt, F., Heald, C., Holland, E. A.,  
1070 Lauritzen, P., and Neu, J.: CAM-chem: Description and evaluation of interactive atmospheric chemistry  
1071 in the Community Earth System Model, *Geoscientific Model Development*, 5, 369-411, 2012.

1072 Lin, C., Cohen, J. B., Wang, S., and Lan, R.: Application of a combined standard deviation and mean  
1073 based approach to MOPITT CO column data, and resulting improved representation of biomass burning  
1074 and urban air pollution sources, *Remote Sensing of Environment*, 241, 111720, 2020a.

1075 Lin, C., Cohen, J. B., Wang, S., Lan, R., and Deng, W.: A new perspective on the spatial, temporal, and  
1076 vertical distribution of biomass burning: quantifying a significant increase in CO emissions,  
1077 *Environmental Research Letters*, 15, 104091, 2020b.

1078 Liousse, C., Guillaume, B., Grégoire, J.-M., Mallet, M., Galy, C., Pont, V., Akpo, A., Bedou, M., Castéra,  
1079 P., and Dungall, L.: Updated African biomass burning emission inventories in the framework of the  
1080 AMMA-IDAF program, with an evaluation of combustion aerosols, *Atmospheric Chemistry and Physics*,  
1081 10, 9631-9646, 2010.

1082 Liu, L., Cheng, Y., Wang, S., Wei, C., Pöhlker, M. L., Pöhlker, C., Artaxo, P., Shrivastava, M., Andreae,  
1083 M. O., and Pöschl, U.: Impact of biomass burning aerosols on radiation, clouds, and precipitation over  
1084 the Amazon: relative importance of aerosol–cloud and aerosol–radiation interactions, *Atmospheric  
1085 Chemistry and Physics*, 20, 13283-13301, 2020a.

1086 Liu, T., Mickley, L. J., Marlier, M. E., DeFries, R. S., Khan, M. F., Latif, M. T., and Karambelas, A.:  
1087 Diagnosing spatial biases and uncertainties in global fire emissions inventories: Indonesia as regional  
1088 case study, *Remote Sensing of Environment*, 237, 111557, 2020b.

1089 Liu, X., Ma, P.-L., Wang, H., Tilmes, S., Singh, B., Easter, R., Ghan, S., and Rasch, P.: Description and  
1090 evaluation of a new four-mode version of the Modal Aerosol Module (MAM4) within version 5.3 of the  
1091 Community Atmosphere Model, *Geoscientific Model Development*, 9, 505-522, 2016.

1092 Liu, Y., Zhang, K., Qian, Y., Wang, Y., Zou, Y., Song, Y., Wan, H., Liu, X., and Yang, X.-Q.: Investigation  
1093 of short-term effective radiative forcing of fire aerosols over North America using nudged hindcast  
1094 ensembles, *Atmospheric Chemistry and Physics*, 18, 31-47, 2018.

1095 McMeeking, G. R., Kreidenweis, S. M., Baker, S., Carrico, C. M., Chow, J. C., Collett Jr, J. L., Hao, W.  
1096 M., Holden, A. S., Kirchstetter, T. W., and Malm, W. C.: Emissions of trace gases and aerosols during  
1097 the open combustion of biomass in the laboratory, *Journal of Geophysical Research: Atmospheres*, 114,  
1098 2009.

1099 Mieville, A., Granier, C., Liousse, C., Guillaume, B., Mouillot, F., Lamarque, J.-F., Grégoire, J.-M., and  
1100 Pétron, G.: Emissions of gases and particles from biomass burning during the 20th century using satellite  
1101 data and an historical reconstruction, *Atmospheric Environment*, 44, 1469-1477, 2010.

1102 Neu, J. and Prather, M.: Toward a more physical representation of precipitation scavenging in global  
1103 chemistry models: cloud overlap and ice physics and their impact on tropospheric ozone, *Atmospheric  
1104 Chemistry and Physics*, 12, 3289-3310, 2012.

1105 Olson, D. M., Dinerstein, E., Wikramanayake, E. D., Burgess, N. D., Powell, G. V., Underwood, E. C.,  
1106 D'amico, J. A., Itoua, I., Strand, H. E., and Morrison, J. C.: Terrestrial Ecoregions of the World: A New  
1107 Map of Life on Earth A new global map of terrestrial ecoregions provides an innovative tool for  
1108 conserving biodiversity, *BioScience*, 51, 933-938, 2001.

1109 Page, S. E., Siegert, F., Rieley, J. O., Boehm, H.-D. V., Jaya, A., and Limin, S.: The amount of carbon  
1110 released from peat and forest fires in Indonesia during 1997, *Nature*, 420, 61-65, 2002.

1111 Pan, X., Ichoku, C., Chin, M., Bian, H., Darmenov, A., Colarco, P., Ellison, L., Kucsera, T., da Silva, A.,  
1112 and Wang, J.: Six global biomass burning emission datasets: intercomparison and application in one  
1113 global aerosol model, *Atmospheric Chemistry and Physics*, 20, 969-994, 2020.

1114 Paton-Walsh, C., Emmons, L. K., and Wiedinmyer, C.: Australia's Black Saturday fires—Comparison of  
1115 techniques for estimating emissions from vegetation fires, *Atmospheric Environment*, 60, 262-270, 2012.

1116 Paton - Walsh, C., Deutscher, N. M., Griffith, D., Forgan, B., Wilson, S., Jones, N., and Edwards, D.:  
1117 Trace gas emissions from savanna fires in northern Australia, *Journal of Geophysical Research:  
1118 Atmospheres*, 115, 2010.

1119 Platnick, S., King, M., Meyer, K., Wind, G., Amarasinghe, N., Marchant, B., Arnold, G., Zhang, Z.,  
1120 Hubanks, P., and Ridgway, B.: MODIS atmosphere L3 monthly product, NASA MODIS Adaptive  
1121 processing system, goddard space flight center, USA, 20, 2015.

1122 [Pokhrel, R. P., Gordon, J., Fiddler, M. N., Bililign, S.: Impact of combustion conditions on physical and  
1123 morphological properties of biomass burning aerosol, \*Aerosol Science and Technology\*, 55\(1\), 80-91,  
1124 2021.](#)

1125 Ramnarine, E., Kodros, J. K., Hodshire, A. L., Lonsdale, C. R., Alvarado, M. J., and Pierce, J. R.: Effects  
1126 of near-source coagulation of biomass burning aerosols on global predictions of aerosol size distributions  
1127 and implications for aerosol radiative effects, *Atmospheric Chemistry and Physics*, 19, 6561-6577, 2019.

1128 Randerson, J. T., van der Werf, G. R., Giglio, L., Collatz, G. J., and Kasibhatla, P. S.: Global Fire  
1129 Emission Database, Version 4.1 (GFEDv4). ORNLDAAC, Oak Ridge, Tennessee, USA, 2018.  
1130 <https://doi.org/10.3334/ORNLDAAAC/1293>

1131 Reid, W. V. and Mooney, H. A.: The Millennium Ecosystem Assessment: testing the limits of  
1132 interdisciplinary and multi-scale science, *Current Opinion in Environmental Sustainability*, 19, 40-46,  
1133 2016.

1134 Reid, W. V., Mooney, H. A., Cropper, A., Capistrano, D., Carpenter, S. R., Chopra, K., Dasgupta, P.,  
1135 Dietz, T., Duraiappah, A. K., and Hassan, R.: *Ecosystems and human well-being-Synthesis: A report of  
1136 the Millennium Ecosystem Assessment*, Island Press, 2005.

1137 Roy, D. P., Boschetti, L., Justice, C., and Ju, J.: The collection 5 MODIS burned area product—Global  
1138 evaluation by comparison with the MODIS active fire product, *Remote sensing of Environment*, 112,  
1139 3690-3707, 2008.

1140 ~~Schaefer, K., Collatz, G. J., Tans, P., Denning, A. S., Baker, I., Berry, J., Prihodko, L., Suits, N., and  
1141 Philpott, A.: Combined simple biosphere/Carnegie – Ames – Stanford approach terrestrial carbon cycle  
1142 model, *Journal of Geophysical Research: Biogeosciences*, 113, 2008.~~

1143 Spracklen, D., Jimenez, J., Carslaw, K., Worsnop, D., Evans, M., Mann, G., Zhang, Q., Canagaratna, M.,  
1144 Allan, J., and Coe, H.: Aerosol mass spectrometer constraint on the global secondary organic aerosol  
1145 budget, *Atmospheric Chemistry and Physics*, 11, 12109-12136, 2011.

1146 Stockwell, T., Zhao, J., Greenfield, T., Li, J., Livingston, M., and Meng, Y.: Estimating under - and  
1147 over - reporting of drinking in national surveys of alcohol consumption: identification of consistent  
1148 biases across four English - speaking countries, *Addiction*, 111, 1203-1213, 2016.

1149 Tilmes, S., Hodzic, A., Emmons, L., Mills, M., Gettelman, A., Kinnison, D. E., Park, M., Lamarque, J.  
1150 F., Vitt, F., and Shrivastava, M.: Climate forcing and trends of organic aerosols in the Community Earth  
1151 System Model (CESM2), *Journal of Advances in Modeling Earth Systems*, 11, 4323-4351, 2019.

1152 Urbanski, S., Hao, W., and Nordgren, B.: The wildland fire emission inventory: western United States  
1153 emission estimates and an evaluation of uncertainty, *Atmospheric Chemistry and Physics*, 11, 12973-  
1154 13000, 2011.

1155 van der Werf, G., Randerson, J., Giglio, L., Collatz, J., Kasibhatla, P., Morton, D., and DeFries, R.: The  
1156 improved Global Fire Emissions Database (GFED) version 3: contribution of savanna, forest,  
1157 deforestation, and peat fires to the global fire emissions budget, *EGU General Assembly Conference  
1158 Abstracts*, 2010a.

1159 van der Werf, G. R., Randerson, J. T., Giglio, L., Collatz, G. J., Kasibhatla, P. S., and Arellano Jr, A. F.:  
1160 Interannual variability in global biomass burning emissions from 1997 to 2004, *Atmospheric Chemistry  
1161 and Physics*, 6, 3423-3441, 2006.

1162 van der Werf, G. R., Randerson, J. T., Giglio, L., Collatz, G., Mu, M., Kasibhatla, P. S., Morton, D. C.,  
1163 DeFries, R., Jin, Y. v., and van Leeuwen, T. T.: Global fire emissions and the contribution of deforestation,  
1164 savanna, forest, agricultural, and peat fires (1997–2009), *Atmospheric chemistry and physics*, 10, 11707-  
1165 11735, 2010b.

1166 van der Werf, G. R., Randerson, J. T., Giglio, L., van Leeuwen, T. T., Chen, Y., Rogers, B. M., Mu, M.,  
1167 van Marle, M. J., Morton, D. C., and Collatz, G. J.: Global fire emissions estimates during 1997–2016,  
1168 *Earth System Science Data*, 9, 697-720, 2017.

1169 Vetrina, Y., Cochrane, M. A., Priyatna, M., Sukowati, K. A., and Khomarudin, M. R.: Evaluating accuracy  
1170 of four MODIS-derived burned area products for tropical peatland and non-peatland fires, *Environmental  
1171 Research Letters*, 16, 035015, 2021.

1172 Warner, J. X., Gille, J. C., Edwards, D. P., Ziskin, D. C., Smith, M. W., Bailey, P. L., and Rokke, L.:  
1173 Cloud detection and clearing for the Earth Observing System Terra satellite Measurements of Pollution  
1174 in the Troposphere (MOPITT) experiment, *Applied Optics*, 40, 1269-1284, 2001.

1175 Webb, M. J., Andrews, T., Bodas-Salcedo, A., Bony, S., Bretherton, C. S., Chadwick, R., Chepfer, H.,  
1176 Douville, H., Good, P., and Kay, J. E.: The cloud feedback model intercomparison project (CFMIP)  
1177 contribution to CMIP6, *Geoscientific Model Development*, 10, 359-384, 2017.

1178 Westerling, A. L. and Bryant, B.: Climate change and wildfire in California, *Climatic Change*, 87, 231-  
1179 249, 2008.

1180 Westerling, A. L., Hidalgo, H. G., Cayan, D. R., and Swetnam, T. W.: Warming and earlier spring increase  
1181 western US forest wildfire activity, *science*, 313, 940-943, 2006.

1182 Wiedinmyer, C., Akagi, S., Yokelson, R. J., Emmons, L., Al-Saadi, J., Orlando, J., and Soja, A.: The Fire  
1183 INventory from NCAR (FINN): A high resolution global model to estimate the emissions from open  
1184 burning, *Geoscientific Model Development*, 4, 625-641, 2011.

1185 Wiedinmyer, C., Quayle, B., Geron, C., Belote, A., McKenzie, D., Zhang, X., O'Neill, S., and Wynne,  
1186 K. K.: Estimating emissions from fires in North America for air quality modeling, *Atmospheric  
1187 Environment*, 40, 3419-3432, 2006.

1188 Williams, J. E., van Weele, M., van Velthoven, P. F., Scheele, M. P., Lioussé, C., and van Der Werf, G.  
1189 R.: The impact of uncertainties in African biomass burning emission estimates on modeling global air  
1190 quality, long range transport and tropospheric chemical lifetimes, *Atmosphere*, 3, 132-163, 2012.

1191 Yang, Y., Smith, S. J., Wang, H., Mills, C. M., and Rasch, P. J.: Variability, timescales, and nonlinearity  
1192 in climate responses to black carbon emissions, *Atmospheric Chemistry and Physics*, 19, 2405-2420,  
1193 2019.

1194 Yokelson, R. J., Susott, R., Ward, D. E., Reardon, J., and Griffith, D. W. T.: Emissions from smoldering  
1195 combustion of biomass measured by open-path Fourier transform infrared spectroscopy, *Journal of  
1196 Geophysical Research: Atmospheres*, 102(D15), 18865-18877, 1997.

1197 Yu, P., Toon, O. B., Bardeen, C. G., Zhu, Y., Rosenlof, K. H., Portmann, R. W., Thornberry, T. D., Gao,  
1198 R.-S., Davis, S. M., and Wolf, E. T.: Black carbon lofts wildfire smoke high into the stratosphere to form  
1199 a persistent plume, *Science*, 365, 587-590, 2019.

1200 Zhang, Y., Li, Z., Chen, Y., de Leeuw, G., Zhang, C., Xie, Y., and Li, K.: Improved inversion of aerosol  
1201 components in the atmospheric column from remote sensing data, *Atmospheric Chemistry and Physics*,  
1202 20, 12795-12811, 2020.

1203

**1204 Table 1. Brief introduction of four BB inventories**

Inventory	“Bottom-up”		“Top-down”	
	FINN1.5	GFED4s	QFED2.5	VFEI0
Temporal range	2002- (NRT) <sup>a</sup>	1997-2022 <sup>b</sup>	2000- (NRT) <sup>a</sup>	2012- (NRT) <sup>a</sup>
Spatio-temporal resolution	1km, daily	0.25°, monthly (daily fraction)	0.1°, daily (0.25° × 0.375°, NRT <sup>a</sup> )	500m, daily
Primary satellite fire input	MCD14DL C5 active fire area (1km)	MCD64A1 C5.1 burned area (500m)	MOD14/MYD14 C6 FRP (1km)	VNP14IMG FRP (1km)
Statistical boosts/Adjustment	Smooth assumption in tropics <sup>c</sup>	Small fire boost (MOD14A1/MYD14A1)	Cloud-gap adjusted FRP density	
Primary land use/land cover (LULC)	MCD12Q1 (IGBP), 2005	MCD12Q1 (UMD), 2001-2012	IGBP-INPE	MCD12C1(IGBP) + The Köppen Climate Classification
Peatland fire	×	Olson et al. (2001)	×	Ferrada et al. (2022)
Conversion to dry matter	Hoelzemann et al. (2004)	CASA biogeochemical model (van der Werf et al., 2010)	QFED FRP vs GFED2 dry matter global calibration	VFEI FRP vs GFED3.1 dry matter global calibration
Emission factors	Akagi et al. (2011), Andreae and Merlet (2001)	Akagi et al. (2011) + updates from Andreae et al. (2013)	Andreae and Merlet (2001), Akagi et al. (2011) <sup>d</sup>	Akagi et al. (2019)
Speciation	41 species	27 species	17 species	46 species
References	Wiedinmyer et al. (2011)	van der Werf et al. (2017)	Darmenov and da Silva (2015)	Ferrada et al. (2022)

1205 a: NRT = near real time; b: 2017-2022 are beta version releases;

1206 c: In equatorial region (30°N-30°S), each detected fire will be counted as 2-day, assuming the second day’s fire will continue to be half the  
1207 size of the previous day;

1208 d: Particulate matter-related emissions from biomass burning (e.g. BC, OC, NH<sub>3</sub>, SO<sub>2</sub>, and PM<sub>2.5</sub>) were corrected from emission factors  
1209 based on MODIS AOD.

1210

1211

1212

1213 **Table 2. CO and OC emission factors used in the four biomass burning emission inventories.**

Emission factors across inventories and vegetation types (g species per kg dry matter)								
Types	CO				OC			
	FINN1.5	GFED4s	QFED2.5	VFEI0	FINN1.5	GFED4s	QFED2.5	VFEI0
Temperate forest	108 <sup>Ak</sup>	88 <sup>Ak</sup>	107 <sup>AM</sup>	113 <sup>An</sup>	6.97 <sup>AR</sup>	9.6 <sup>AM</sup>	41.09 <sup>*</sup>	10.9 <sup>An</sup>
Boreal forest	118 <sup>Ak</sup>	127 <sup>Ak</sup>	107 <sup>AM</sup>	121 <sup>An</sup>	7.31 <sup>Mc</sup>	9.6 <sup>AM</sup>	41.09 <sup>*</sup>	5.9 <sup>An</sup>
Savanna and Grass, shrub	59 <sup>Ak</sup> /68 <sup>Ak</sup>	63 <sup>Ak</sup>	65 <sup>AM</sup>	69 <sup>An</sup>	2.6 <sup>Ak</sup> /6.61 <sup>Mc</sup>	2.62 <sup>Ak</sup>	6.12 <sup>*</sup>	3 <sup>An</sup>
Tropical forest	92 <sup>Ak</sup>	93 <sup>Ak</sup>	104 <sup>AM</sup>	104 <sup>An</sup>	4.77 <sup>Ak</sup>	4.71 <sup>Ak</sup>	13 <sup>*</sup>	4.4 <sup>An</sup>
Agricultural	111 <sup>Ak</sup>	102 <sup>Ak</sup>	/	76 <sup>An</sup>	3.3 <sup>AM</sup>	2.3 <sup>Ak</sup>	/	4.9 <sup>An</sup>
Peatlands	/	210 <sup>#</sup>	/	260 <sup>An</sup>	/	6.02 <sup>#</sup>	/	14.2 <sup>An</sup>

1214 Ak: Akagi et al. (2011); AM: Andreae and Merlet (2001); An: Andreae (2019); AR: Andreae and Rosenfeld (2008); Mc: McMeeking et al. (2009)

1215 \*: QFED2.5 PM-related emission factors are obtained by multiplying the base EF multiplied by its biome-specific enhancement factor

1216 #: Emission factors for peatland is the average of lab measurements of Yokelson et al. (1997) and Christian et al. (2003)

1217

1218



1219 **Table 3. Comparison of CESM-CAM6 simulated CO column averages and satellite retrieved CO**  
 1220 **column averages during the fire season.**

Regions	Fire- Season	Satellite		CESM2-CAM6		
		MOPITT	FINN1.5	GFED4s	QFED2.5	VFEI0
EQAS	Jan.-Apr.	1.88	1.66	<i>1.69</i>	1.61	1.47
BONA	Apr.-Aug.	2.03	1.29	<i>1.47</i>	1.30	1.32
SEAS	Feb.-Apr.	2.40	<i>2.10</i>	1.94	1.89	1.95
SHAF	May.-Nov.	2.31	1.75	2.04	1.99	<i>2.19</i>
NHAF	Jan.-May.	2.66	1.96	2.02	2.05	<i>2.10</i>
BOAS	Mar.-Nov.	2.05	1.31	<i>1.42</i>	1.33	1.34
SHSA	July.-Dec.	1.77	<i>1.75</i>	<i>1.80</i>	<i>1.76</i>	<i>1.80</i>

1221  
 1222

1223 **Table 4. Same as Table 3 but for AOD**

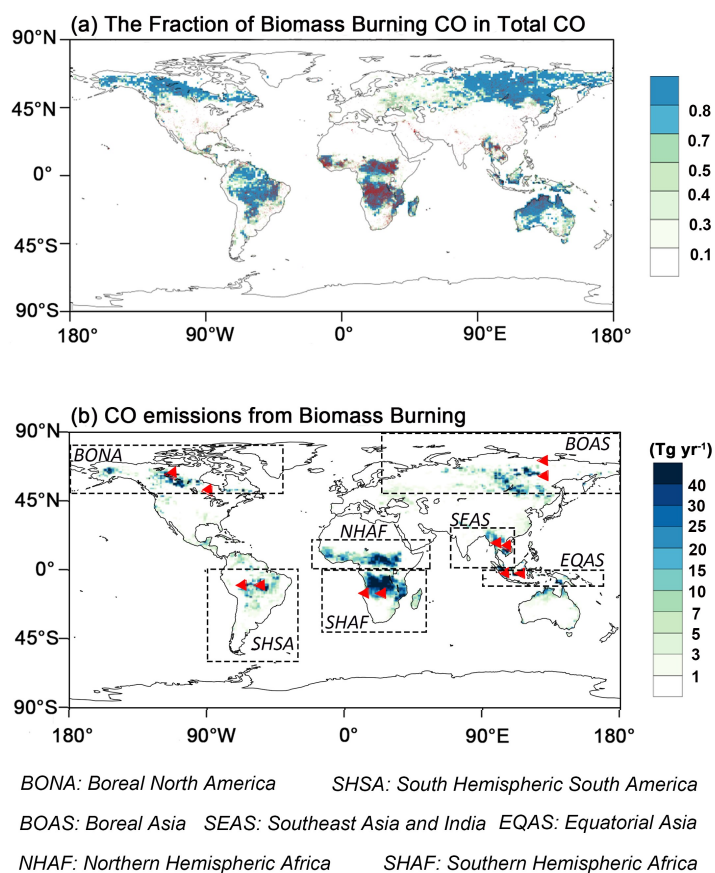
Regions	Satellite		CESM2-CAM6		
	MODIS	FINN1.5	GFED4s	QFED2.5	VFEI0
EQAS	0.23	<i>0.22</i>	<i>0.25</i>	<i>0.23</i>	<i>0.21</i>
BONA	0.13	0.07	<i>0.12</i>	<i>0.11</i>	0.07
SEAS	0.30	0.35	<i>0.30</i>	0.36	<i>0.30</i>
SHAF	0.33	<i>0.31</i>	<i>0.37</i>	0.53	<i>0.40</i>
NHAF	0.32	<i>0.53</i>	0.54	0.61	0.55
BOAS	0.15	0.11	<i>0.13</i>	<i>0.16</i>	0.11
SHSA	0.14	0.30	0.31	0.34	<i>0.29</i>

1224

1225

1226

1227



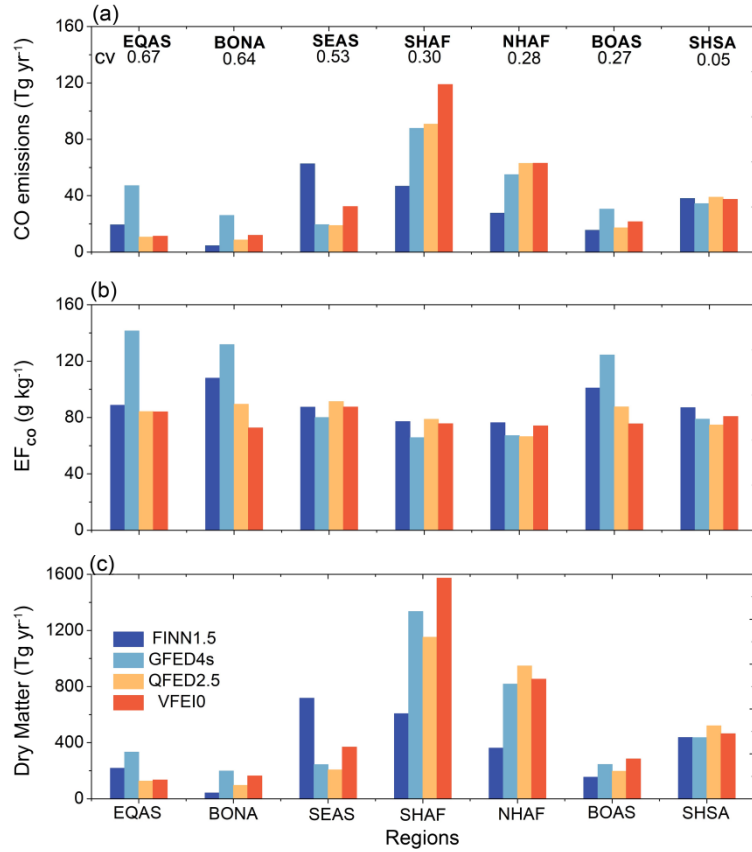
1228

1229 **Figure 1.** (a) The fraction of BB CO emissions to the sum of anthropogenic and BB CO emissions  
1230 (CO\_BB/CO\_Total) during 2013-2016 and (b) the spatial distribution of CO emissions (FINN1.5 was  
1231 used as an example). The red dots in Fig. 1(a) are the fire points from the MCD14DL satellite product.  
1232 In Fig. 1(b), seven regions with high BB emissions taken from those applied by van der Werf et al. (2006,  
1233 2010) are marked with black boxes, and the red triangles represent 12 AERONET stations. In this study,  
1234 seven major BB regions includes Boreal North America (BONA), Boreal Asia (BOAS), Southeast Asia  
1235 (SEAS), Equatorial Asia (EQAS), North Hemisphere Africa (NHAF), South Hemisphere Africa (SHAF),  
1236 and South Hemisphere South America (SHSA).

1237

1238

1239



1240

1241 **Figure 2.** (a) Average annual CO emissions of four biomass burning emission inventories across seven  
 1242 major BB regions during 2013-2016. The cv, defined as the ratio of the standard deviation to the mean,  
 1243 is the coefficient of variation among the emissions of four datasets. (b) and (c) are the same as (a), but  
 1244 for the emission factor of CO (EF<sub>CO</sub>) and Dry Matter.

1245

1246

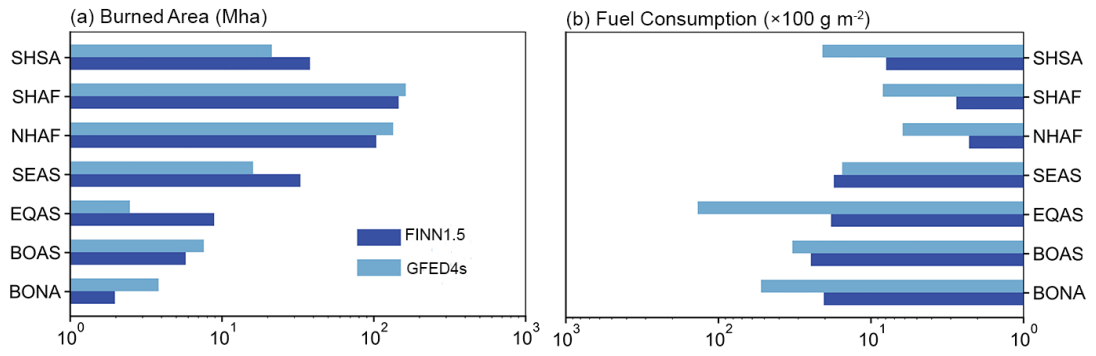
1247

1248

1249

1250

1251



1252

1253

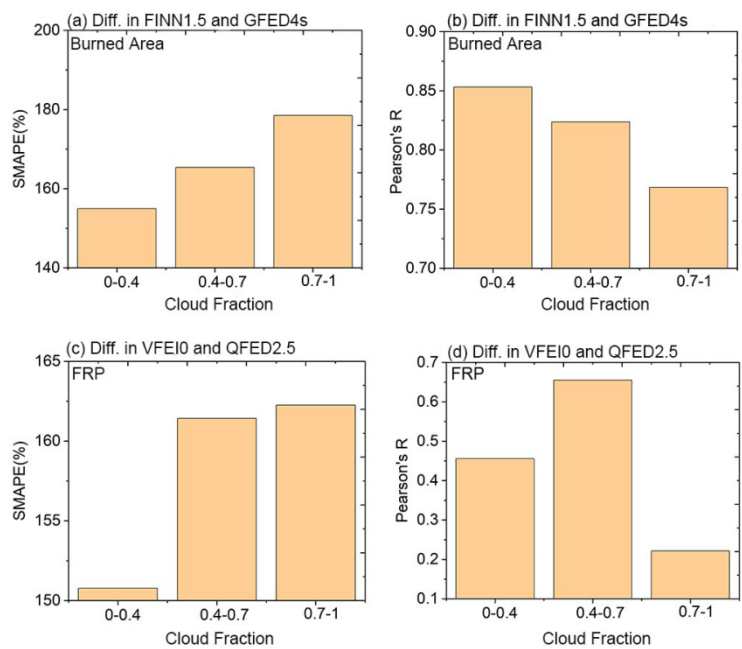
**Figure 3.** Annual burned area (a) and fuel consumption (b) of two bottom-up datasets (FINN1.5 and GFED4s) across seven regions from 2013 to 2016.

1254

1255

1256

1257



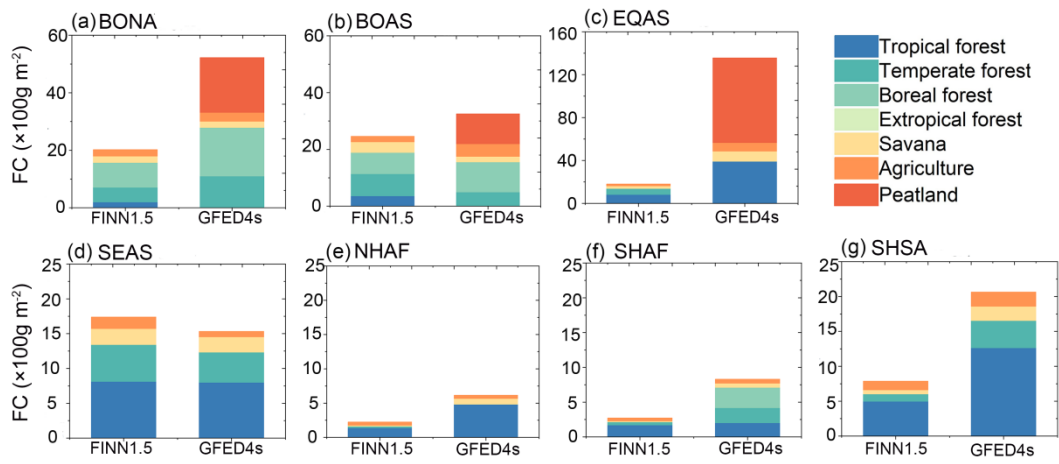
1258

1259 **Figure 4.** The differences in (a-b) burned areas and (c-d) total FRP detected by two inventories under  
1260 different cloud fraction in a pilot region of BONA. These differences are quantified by two indicators:  
1261 SMAPE and Pearson's R. Cloud fraction data is calculated from MODIS product MCD06COSP.

1262

1263

1264



1265

1266

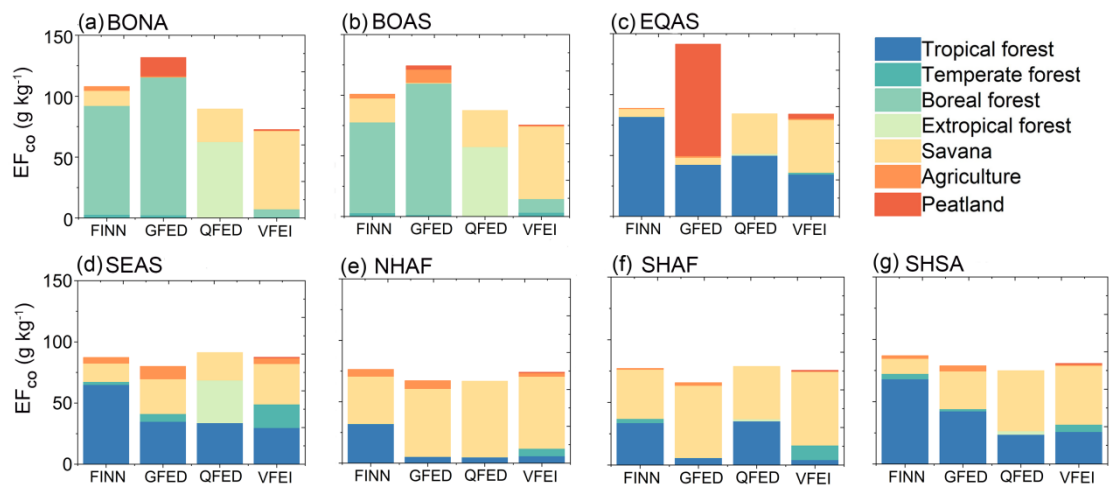
1267

1268

1269

**Figure 5.** Annual average fuel consumption of two bottom-up datasets (FINN1.5 and GFED4s) across seven regions from 2013 to 2016. The contributions of the seven biomes are shown in different colors.

1270



1271

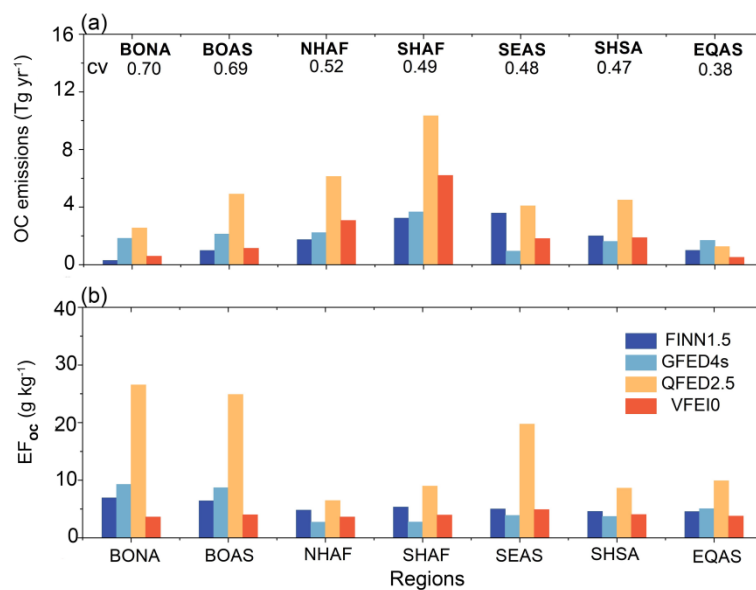
1272 **Figure 6.** Regional comprehensive emission factors for four datasets (FINN1.5, GFED4s, QFED2.5,  
1273 and VFEI0) in seven regions from 2013 to 2016. The contributions of the seven biomes are shown in  
1274 different colors.

1275

1276



1277



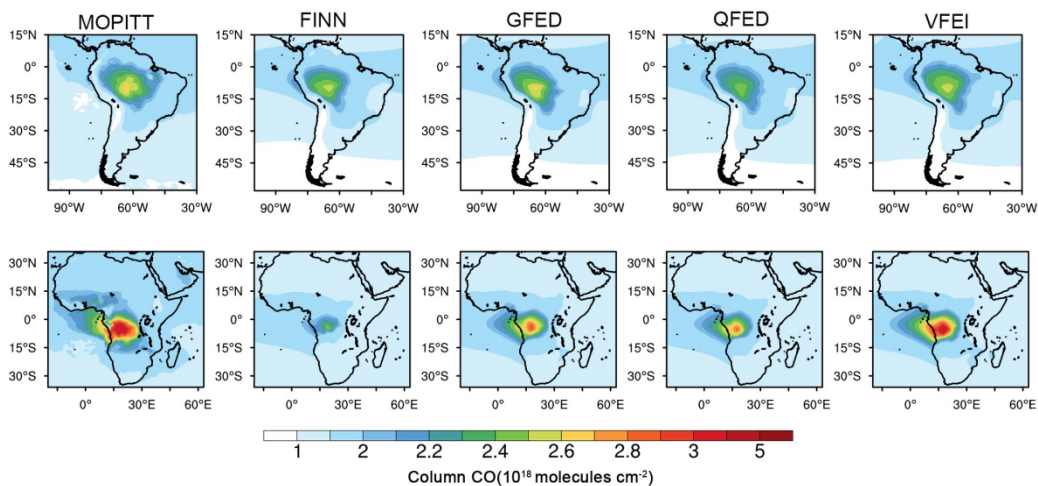
1278

1279 **Figure 7.** (a) Average annual OC emissions of four biomass burning emissions inventories across seven  
1280 major BB regions during 2013-2016. The cv, defined as the ratio of the standard deviation to the mean,  
1281 is the coefficient of variation among the emissions of four datasets. (b) is the same as (a) but for the  
1282 emission factor of OC (EF<sub>oc</sub>).

1283

1284

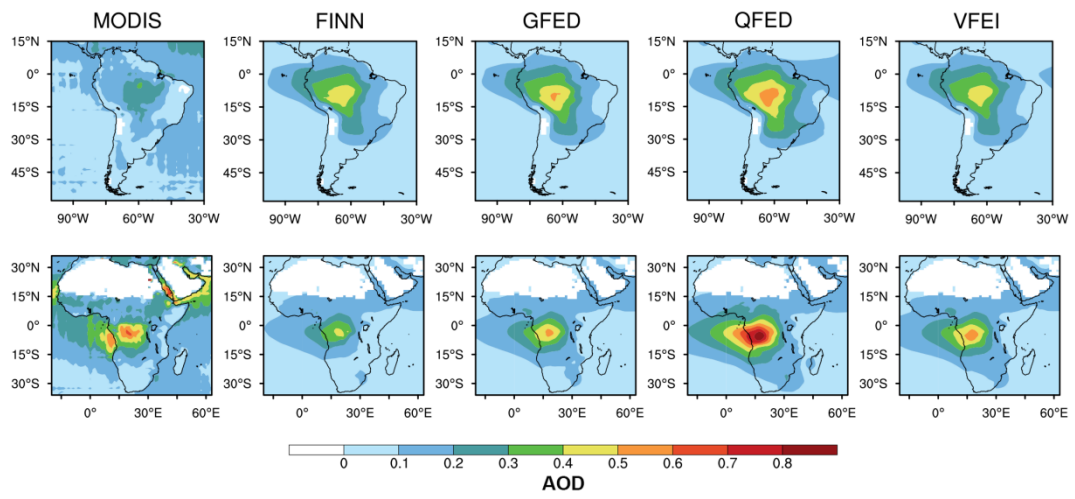
1285



1286

1287 **Figure 8.** Spatial distribution of CO column burdens from MOPITT and CESM2-CAM6 simulations  
1288 during the fire season (Table 3). The text above each plot identifies the name of the satellite inversion  
1289 dataset or emission inventory dataset applied by the model, namely FINN1.5, GFED4s, QFED2.5, and  
1290 VFEI0.  
1291

1292



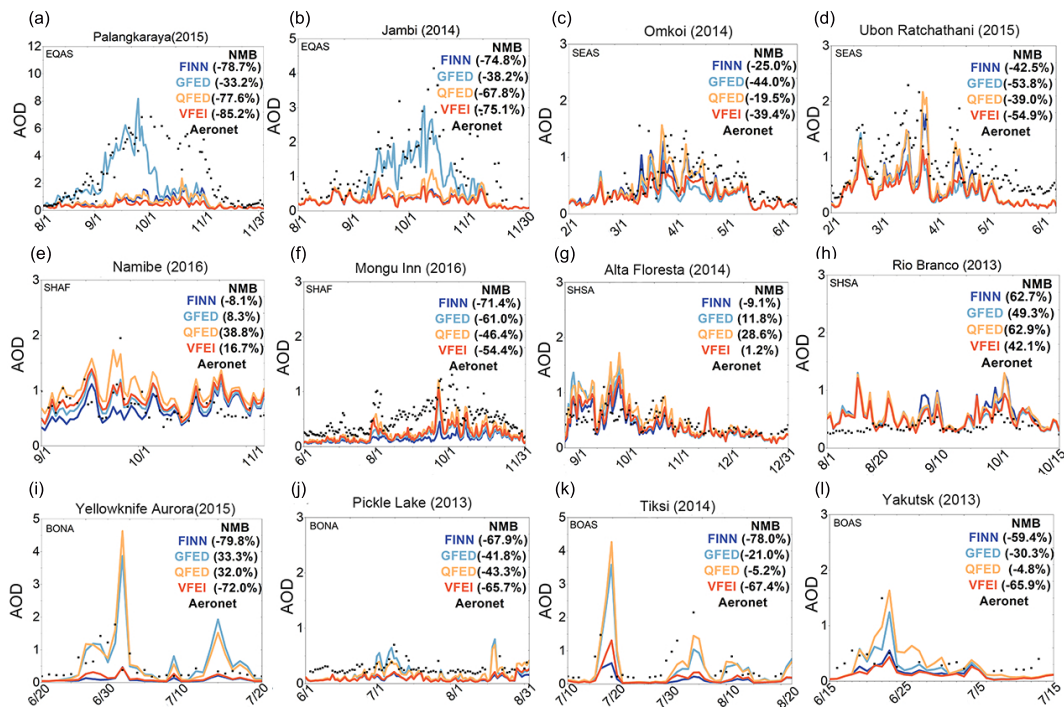
1293

1294

**Figure 9.** The same as figure 8 but for AOD.

1295

1296



1298

1299

1300

1301

1302

1303

1304

1305

1306

**Figure 10.** Comparison between AOD simulated by CESM2-CAM6 using the four datasets (FINN1.5, GFED4s, QFED2.5, and VFEI0) and AERONET ground-based observations during fire seasons. These AERONET sites are: (a) Palangkaraya (2.2°S, 113.9°E), (b) Jambi (1.6°S, 103.6°E), (c) Omkoi (17.8°N, 98.4°E), (d) Ubon Ratchathani (15.2°N, 104.9°E), (e) Namibe (15.2°S, 12.2°E), (f) Mongu Inn (15.3°S, 23.1°E), (g) Alta Floresta (9.9°S, 56.1°W), (h) Rio Branco (9.9°S, 67.9°W), (i) Yellowknife\_Aurora (62.5°N, 114.4°W), (j) Pickle Lake (51.4°N, 90.2°W), (k) Tiksi (71.6°N, 128.9°E), (l) Yakutsk (61.7°N, 129.4°E).